Journal of Hydrology 627 (2023) 130454

Contents lists available at ScienceDirect

Journal of Hydrology

journal homepage: www.elsevier.com/locate/jhydrol

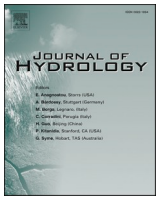

Research papers

Spatial and temporal patterns of agricultural drought in China during 1960–2020 characterized by use of the crop water deficit Abnormal Index

Ning Jin [a], Yu Shi [b,c,*], Wenhao Niu [b], Liang He [d,*]

[a] Department of Resources and Environment, Shanxi Institute of Energy, Jinzhong 030600, China
[b] State Key Laboratory of Soil Erosion and Dryland Farming on the Loess Plateau, College of Natural Resources and Environment, Northwest A&F University, Yangling, Shaanxi 712100, China
[c] International Center for Climate and Global Change Research, College of Forestry, Wildlife and Environment, Auburn University, Auburn, AL 36849, USA
[d] National Meteorological Center, Beijing 100081, China

ARTICLE INFO

This manuscript was handled by Y. Huang, Editor-in-Chief, with the assistance of Shanshui Yuan, Associate Editor

Keywords:
Drought duration
Drought severity
Site observations
Crop water deficit abnormal index

ABSTRACT

Agricultural drought intensifies crop water stress and limits photosynthetic productivity, thereby threatening food security and socio-economic development. However, current drought indices from model simulations or remote sensing have limitations with regard to fully considering the complex interactions between various climate factors and crop water demands. Furthermore, estimates from remote sensing-based drought indices are subject to significant uncertainties due to the coarse spatiotemporal resolution of the data sources, inherent systematic errors in methodologies, and the limited number of ground observations. This study aimed to bridge these gaps by employing the nationwide Agricultural Drought Monitoring Network covering over 2000 in-situ observations and the Crop Water Deficit Abnormal Index (*CWDIa*) to quantify the spatiotemporal characteristics of agricultural drought from 1960 to 2020. The duration and severity of drought in northern China were significantly greater than in the southern regions, especially in the North China Plain, and the northern Tibetan Plateau. The occurrence of severe drought in southwestern China and in the southern Tibetan Plateau during the spring and winter seasons was driven by persistent water deficits. Over the past 60 years, China has experienced an overall alleviation in the severity and duration of agricultural drought. However, the drought situation has continued to worsen in certain regions, such as in southwestern China and the southern North China Plain. Multiscale decomposition of the ensemble empirical mode has further strengthened this finding (i.e., the drying trend in southwestern China since 1990). As seen in authoritative drought statistics, the integration of *CWDIa* and dense observations in the drought monitoring framework have demonstrated robust efficacy in capturing over 80 % of the actual drought-covered and drought-affected area. These findings highlight the importance of incorporating climate and crop water demand in agricultural drought monitoring to provide reliable and long-term spatiotemporal estimates of drought characteristics based on a nationwide observation network.

1. Introduction

Drought is one of several extreme weather events that has become more frequent than ever before due to climate change occurring over most of world, even in wet or humid regions (Mishra and Singh, 2010; Dai, 2011). Extreme drought has profound impacts on agriculture, water resources, the ecosystem carbon cycle, and socio-economic development (Clarke et al., 2021; Luo and Keenan, 2022; Yin et al., 2023). China is one of the countries currently dealing with significant drought disasters. It has an average annual drought-covered area of 20.9 million hectares and a drought-affected area of 8.87 million hectares (Yu et al., 2014; Zhai et al., 2017; Wang et al., 2023). Annual losses in food production caused by drought range from millions of tons to in excess of 30 million tons (Qin et al., 2014; Shi et al., 2021; Wang et al., 2023). With increasing drought intensity and areal coverage across China, drought losses could double in response to global warming of 1.5 ℃ to 2.0 ℃ (Su et al., 2018). Therefore, drought disaster is a serious threat to food and ecological security, and has become a constraining factor for sustainable socio-economic development in China (Zhang et al., 2020).

There exist a plethora of indices derived from a variety of data-driven

* Corresponding authors at: State Key Laboratory of Soil Erosion and Dryland Farming on the Loess Plateau, College of Natural Resources and Environment, Northwest A&F University, Yangling, Shaanxi 712100, China (Yu Shi); National Meteorological Center, Beijing 100081, China (Liang He).
E-mail addresses: shiyu174274@163.com (Y. Shi), heliang@cma.gov.cn (L. He).

https://doi.org/10.1016/j.jhydrol.2023.130454
Received 30 June 2023; Received in revised form 6 September 2023; Accepted 15 October 2023
Available online 11 November 2023

approaches, theoretical foundations, and model structures that have been used to assess and predict the spatiotemporal evolution of agricultural drought in China, based on meteorology [Standardized Precipitation Index (SPI), Standardized Precipitation Evapotranspiration Index (SPEI), and Palmer Drought Severity Index (PDSI)], soil moisture [Standardized Soil Moisture Index (SSI), hydrology [Standardized Runoff Index], and remote sensing [Vegetation Condition Index] (Palmer, 1965; McKee et al., 1993; Liu and Kogan, 1996; Vicente-Serrano et al., 2010; Rojas et al., 2011; AghaKouchak, 2014; Martínez-Fernández et al., 2015). For example, SPI contains a flexible time scale, but it neglects the influences of temperature and evapotranspiration (McKee et al., 1993). SPEI is an extension of SPI that incorporates precipitation and potential evapotranspiration in determining drought (Vicente-Serrano et al., 2010). PDSI considers not only the current water supply and demand, but also the impact of past dry and wet conditions and their duration. However, meteorological drought may not accurately reflect agricultural drought due to differences in the characteristics of drought indices, the time effect in drought spread, and crop resilience. Hence, researchers have used soil moisture derived from model simulations and remote sensing data to construct agricultural drought indices. However, current spatiotemporally continuous soil moisture datasets inevitably contain significant errors and uncertainties due to systematic biases, challenges related to human management practices, limited station observations, and coarse spatiotemporal resolution. Moreover, the development of drought indices based solely on soil moisture provides only an indirect reflection of agricultural drought characteristics (Zhang et al., 2023). In light of these concerns, there is a crucial need to integrate complex climate factors and crop water demands for accurate monitoring of agricultural drought conditions and for accurate quantification of crop water deficits (Sawada et al., 2014).

Indeed, assessments derived from various drought indices can yield disparate or even contradictory outcomes. For example, Wu et al. (2020) employed SPEI_PM to evaluate drought characteristics in China from 1960 to 2014, and found a wetting trend during this period. Yao et al. (2018) reported consistent findings according to multiple drought indices, revealing an overall alleviation of drought conditions in China from 1961 to 2013. In contrast, Han et al. (2020) analyzed the spatiotemporal pattern of drought in China from 1950 to 2009 using an integrated scPDSI dataset. Their findings showed a slight increase in the intensity of annual and seasonal drought over the past 60 years, particularly in eastern China where dry conditions have become more severe. Even employing an identical drought index does not guarantee consistent drought assessments, as substantial deviations can emerge due to differences in a study's time periods. For instance, an evaluation based on SPEI revealed a drying trend across northwestern China from 1985 to 2018 (Shi et al., 2023). However, an entirely opposite outcome was found when the analysis period was extended to cover the years of 1965 to 2017 (Zeng et al., 2020).

The use of ground-based observations have typically been regarded as the most reliable and accurate method for monitoring agricultural drought (Srivastava, 2017). However, past research has been limited by sparse and unevenly-distributed site observations that have hindered the accurate detection of drought conditions. Although remote sensing and numerical simulations serve as alternatives for large-scale drought monitoring, these methods still struggle to overcome the challenges of low assessment accuracy and limited practical application. To bridge the research gap, the China National Meteorological Center developed the Crop Water Deficit Anomaly Index (*CWDIa*) by combining meteorological drought, anthropogenic management, and crop water demand. They also established a national agricultural drought monitoring service system that consists of a network of over 2000 site observations across China to accurately monitor agricultural drought status.

The overall objective of this study was to quantify agricultural drought characteristics (duration and severity) in China over the past six decades (1960–2020) using long-term observations from a dense drought-monitoring network along with statistical data on drought events. In addition, we used *CWDIa* as a probe to investigate agricultural drought, considering crop water balance under the interactions of climate change and crop water demand. This study addressed the following scientific questions: (1) How have spatial and temporal variations in agricultural drought in China changed as assessed by *CWDIa*? (2) What are the geographic differences in the multiscale characteristics (periodicity and trend) of drought based on long-term and multi-site observations across China? (3) Can the proposed drought evaluation system capture actual drought disasters in a robust and accurate manner?

2. Materials and methods

2.1. Study area

China stands globally as one of the countries with the highest frequency of drought occurrences. Drought characteristics induced by climate change exhibit substantial temporal and regional disparities. Considering the diverse combinations of temperature, precipitation, and solar radiation, the entire nation has been classified into twelve subclimatic zones based on their region-specific climatic features (Fig. 1), including Northeast China (NE), North China (NC), South China (SC), Huanghuai district (HH), Jianghan district (JHA), Jianghuai district (JHI), Jiangnan district (JN), Inner Mongolia (NM), Tibetan Plateau region (QT), East-central Northwest China (CEN), Southwest China (SW), and Xinjiang (XJ) (China Meteorological Administration, 2018).

These sub-regions cover diverse geographical features and the main grain-producing areas across China, such as the wheat-producing regions in the North China Plain, rice-producing regions in northeastern and southern China, corn-producing regions in northwest China, and barley-producing regions on the Qinghai-Tibet Plateau. A dense network of meteorological monitoring stations (totaling 2055 stations) is distributed throughout each of the sub-regions (Fig. 1), spanning the extensive period from 1960 to 2020.

2.2. Crop water deficit Abnormal Index

The Crop Water Deficit Abnormal Index (China Meteorological Administration, 2015) was calculated as:

$$CWDI_a = \begin{cases} \dfrac{CWDI - \overline{CWDI}}{100 - \overline{CWDI}} \times 100\% when \overline{CWDI} > 0 \\ CWDI when \overline{CWDI} \le 0 \end{cases} \quad (1)$$

where $CWDI$ is the crop water deficit index, which is calculated in equation (2); $\overline{CWDI}$ is the average crop water deficit abnormal index during a climatic period (e.g., 1981–2010 would be 30 years), which is defined in equation (3). $CWDI$ is calculated as:

$$CWDI = a \times CWDI_j + b \times CWDI_{j-1} + c \times CWDI_{j-2} + d \times CWDI_{j-3} + e \times CWDI_{j-4} \quad (2)$$

where $CWDI_j$ is the crop water deficit index during the j^{th} period (taken as 1 d), which is calculated in equation (4). $CWDI_{j-1}$, $CWDI_{j-2}$, $CWDI_{j-3}$, $CWDI_{j-4}$ are the crop water deficit indices during the $(j-1)^{th}$, $(j-2)^{th}$, $(j-3)^{th}$, $(j-4)^{th}$, periods, respectively. a, b, c, d, e represent the weight of the coefficient of the crop water anomaly index in different periods. In general, the closer the time period, the larger the weight of the coefficient. In this study, a was 0.3; b was 0.25; c was 0.2; d was 0.15; e was 0.1, with reference to *agricultural drought grade* (China Meteorological Administration, 2015).

The average crop water deficit abnormal index ($\overline{CWDI}$) was expressed as:

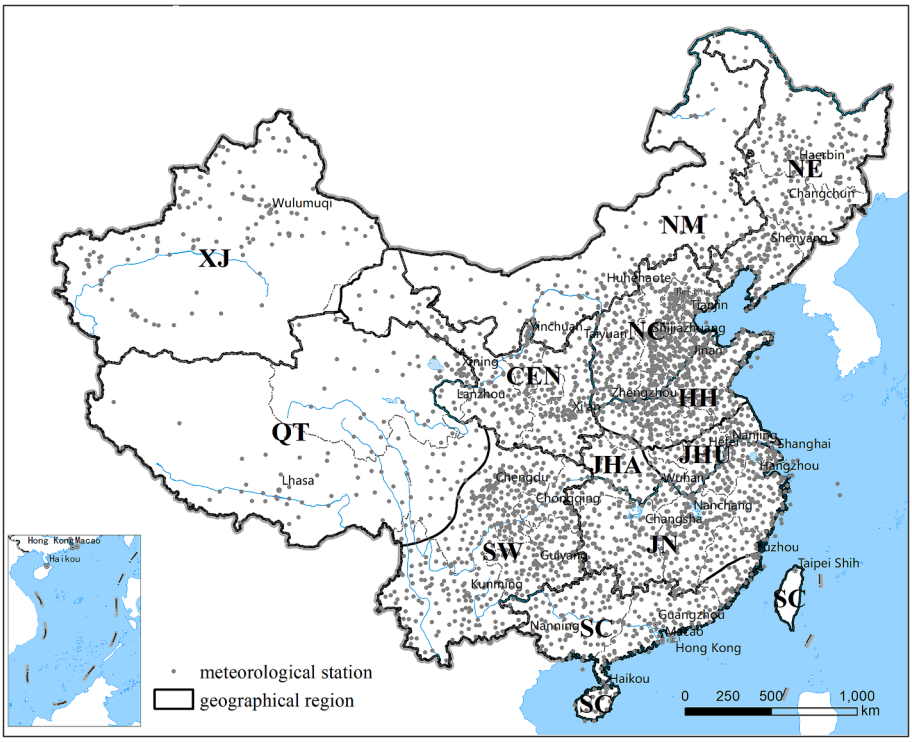

Fig. 1. Meteorological stations and geographical regions. NE: Northeast China; NC: North China; SC: South China; HH: Huanghuai district; JHA: Jianghan district; JHI: Jianghuai district; JN: Jiangnan district; NM: Inner Mongolia; QT: Tibetan Plateau region; CEN: East-central Northwest China; SW: Southwest China; XJ: Xinjiang.

$$\overline{CWDI} = \frac{1}{n}\sum_{i=1}^{n} CWDI_i \tag{3}$$

where n is 30 (the most recent three decades). The crop water deficit index during the j^{th} period ($CWDI_j$) is expressed as:

$$CWDI_j = \left(1 - \frac{P_j + I_i}{ETc_j}\right) \times 100\% \tag{4}$$

where P_j is the accumulated precipitation (mm) during the j^{th} period; I_i is the irrigation amount (mm) during the j^{th} period; ETc_j is the crop potential evaporation (mm), calculated as:

$$ETc_j = K_c ET_0 \tag{5}$$

where K_c is the crop coefficient, which was the average crop coefficient during a given period in a specific region. Detailed K_c values for each province are shown in Appendix A. ET_0 (mm day^{-1}) is the reference crop evapotranspiration as defined by FAO (Allen et al., 1998). The specific equation is:

$$ET_0 = \frac{0.408\Delta(R_n - G) + \gamma u_2(e_s - e_a)[900/(T+273)]}{\Delta + \gamma(1 + 0.34u_2)} \tag{6}$$

where T is mean daily air temperature at 2 m height (°C); R_n is net radiation (MJ m^{-2} day^{-1}); G is soil heat flux density (MJ m^{-2} day^{-1}); u_2 is wind speed at 2 m height (m s^{-1}); e_s and e_a are saturation vapor pressure and actual vapor pressure, respectively (kPa); Δ is the slope of the vapor pressure–temperature curve (kPa °C^{-1}); and γ is the psychrometric constant (kPa °C^{-1}).

The drought classifications based on $CWDI_a$ are given in the Table 1. Notably, we assumed rainfed conditions for the entire study area due to the limited amount of irrigation data at the site scale and the inherent uncertainty associated with irrigation maps. This assumption implies that $CWDI_a$ may overestimate or underestimate the capturing of agricultural drought characteristics in irrigated regions to some extent. Further elaboration on this issue will be provided in the Discussion section.

Table 1
Drought classifications of Crop Water Deficit Abnormal Index ($CWDI_a$).

Drought classification	$CWDI_a$ (%)
Normal	$CWDI_a \leq 40$
Mild drought	$40 < CWDI_a \leq 55$
Moderate drought	$55 < CWDI_a \leq 70$
Severe drought	$70 < CWDI_a \leq 85$
Extreme drought	$CWDI_a > 85$

2.3. Drought severity and duration

Run theory (Yevjevich, 1967) was used to define the drought events as shown in Fig. 2. A drought event started when daily $CWDI_a$ was above the drought threshold (40 % in the Table 1), and ended when $CWDI_a$ fell below the threshold value (China Meteorological Administration, 2015). The period between the beginning and ending times was the drought duration. The drought severity of a drought event was defined as the shaded area surrounded by the daily $CWDI_a$ and $CWDI$ threshold lines (Fig. 2). The annual drought duration at a meteorological station was the sum of all drought event durations in a year. Similarly, annual drought severity was the sum of all drought event severities in a year.

2.4. Meteorological and drought disaster survey data

The original meteorological data were obtained for 2419 stations from the National Meteorological Center of the China Meteorological Administration (http://data.cma.cn), including daily mean, maximum, and minimum air temperatures, precipitation, wind speed, relative humidity, and sunshine hours for the period of 1960–2020. Consistent quality control standards were applied to these data. Before performing calculations, data with missing values exceeding 5 % of the total number

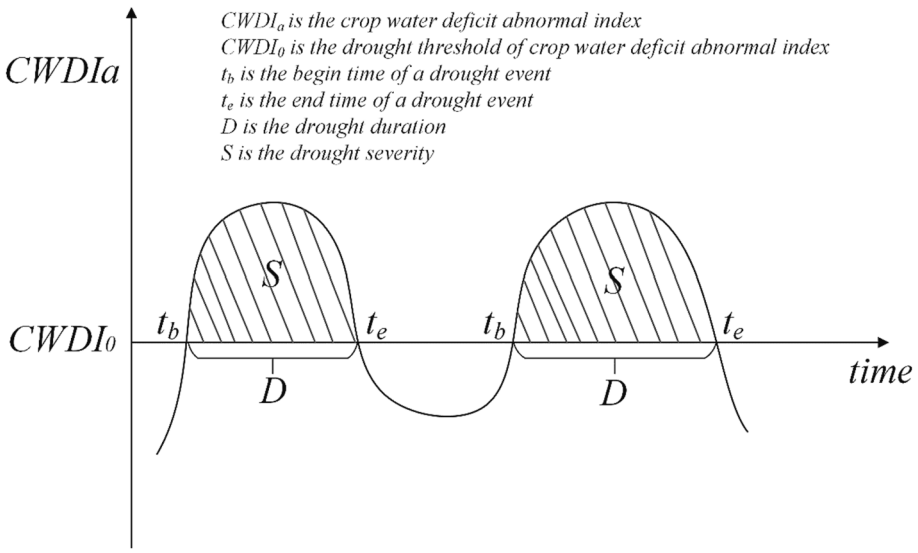

Fig. 2. Drought duration and severity based on the daily Crop Water Deficit Abnormal Index using run theory.

of days were excluded. Moreover, we employed historical data from certain sites to estimate the missing meteorological parameters by calculating average values from corresponding days across different years. Ultimately, 2055 meteorological stations were retained for the computation of drought indices and characteristics (Fig. 1). The area encompassing the stations was divided into twelve geographical regions according to the geographical partition of meteorological products in China (China Meteorological Administration, 2018).

The annual statistics of drought disaster survey data and crop planting areas during 1960 to 2020 (with breaks in 1967–1969) were obtained from the National Bureau of Statistics of China (http://www.stats.gov.cn/) that included national-level drought-covered areas and drought-affected areas. The ratios of drought-covered and drought-affected areas were calculated using disaster survey data divided by crop planting areas.

2.5. Data analysis

Annual drought duration and severity at each station were calculated as described section 2.2. Mean annual, spring, summer, autumn, and winter drought duration and severity at each station were also calculated. The annual drought duration and severity in 12 geographical regions were aggregated by averaging the corresponding stations in each region. We used a non-parametric trend test (i.e., Sen Slope estimator test; (Sen, 1968) to examine the temporal trend at each station and region.

2.6. Emerging hot spot analysis

An Emerging Hot Spot Analysis approach was employed in this study to identify the spatiotemporal trends and clustering features of drought characteristics. Firstly, a space–time cube was created using ArcGIS Pro V3.0 software, in NetCDF format, based on annual drought characteristics (duration and severity) from 1960 to 2020 (for details of the space–time cube see: https://bit.ly/3GZhh8a). Each bin in this cube contained unique identifiers for location, time-step, count values, and aggregated variables produced during the cube's creation (Khoshnazar et al., 2023). Bins associated with the same time-step interval were combined into a time slice. Bins at different time dimensions but the same location were integrated to create a time series containing variable information. We then utilized the emerging hot spot analysis tool in ArcGIS Pro V3.0 to drive the constructed space–time cube and explore spatial clustering distribution and temporal trends of drought characteristics. A non-parametric Mann-Kendall trend test was applied to assess the trend characteristics of the time series. Hence, the outcome of this analysis was a clustering trend z-score, p-value, and binning category for each location. Moreover, based on the spatiotemporal relationships of z-scores and p-values, we further identified cold spots and hot spots in sixteen patterns, comprising eight patterns each for cold spots and hot spots (Scott and Janikas, 2010; Khoshnazar et al., 2023). The pattern names and definitions of hot spot analysis are listed in the Table S2. For additional details and instructions for the Emerging Hot Spot Analysis, please refer to the following link: https://pro.arcgis.com/en/pro-app/latest/tool-reference/space-time-pattern-mining/emerginghotspots.htm.

2.7. Ensemble Empirical mode Decomposition

To obtain the different temporal scales and nonlinear trends in the drought duration and severity series, Empirical Mode Decomposition (EMD) was used. This is an adaptive and efficient method to decompose nonlinear and non-stationary data into several components of intrinsic mode function (IMF) and a residual using a sifting process. This sifting process is described as follows:

Identify the local maxima and minima of the original data $x(t)$. All local maxima are then connected by a cubic spline to form the upper envelope, and minima are connected to form the lower envelope. Their mean is designated as m_1, and the difference between $x(t)$ and m_1 is the first component h_1:

$$h_1 = x(t) - m_1 \tag{7}$$

However, if h_1 does not satisfy the definition of an IMF, then the process is repeated.

$$h_{11} = h_1 - m_{11} \tag{8}$$

where m_{11} is the mean envelope of h_1. Repeat this step k times until h_{1k} is an IMF.

$$h_{1k} = h_{1(k-1)} - m_{1k} \tag{9}$$

Then, the first IMF,$c_1 = h_{1k}$ when

$$D_k = \frac{\sum_{t=0}^{T} |h_{1(k-1)}(t) - h_{1k}(t)|^2}{\sum_{t=0}^{T} |h_{1(k-1)}(t)|^2} \tag{10}$$

where D_k is the stop criterion and smaller than a predetermined value such as 0.2. Once the first IMF is removed from the original

data, $x(t)$

$$r_1 = x(t) - c_1 \tag{11}$$

Because r_1 still contains information of longer period components, it is treated as the new data and subjected to the same sifting process as described above. If c_1 or r_1 is smaller than a predetermined value, or becomes a monotonic function, then the sifting process is stopped. Thus,

$$r_1 = x(t) - c_1, r_2 = x(t) - c_c, \cdots r_n = r_{n-1} - c_n \tag{12}$$

$$x(t) = \sum_{i=1}^{n} c_i + r_n \tag{13}$$

Thus, a series of IMFs can be obtained.

The mode mixing was a significant drawback of EMD, and implied that there was a single IMF consisting of signals of obviously disparate scales or a signal of the same scale appearing in a different IMF component. Wu and Huang (2009) proposed a new noise-assisted analysis method called Ensemble Empirical Mode Decomposition (EEMD) to overcome this problem. The algorithm of EEMD is described as follows:

(1) Add a white noise series to the original signal and decompose the signal with added white noise into IMFs using EMD.

(2) Repeat step (1) but with a different white noise series each time and obtain the corresponding IMF components of the decompositions.

(3) Adopt the means ensemble corresponding to the IMFs and residue of compositions as the final result. The significance of IMF white noise is tested according to the method introduced by Wu and Huang (2004). The variances of each IMF and residual were calculated as variance$(IMF_i)/\sum$variance(IMF_i).

2.8. Drought analysis framework

The drought analysis framework is shown in Fig. 3. Firstly, the $CWDI_a$ for each station from 1961 to 2020 was calculated using daily meteorological data at 2055 stations. Secondly, annual drought duration and severity at each station were assessed by run theory, and the mean drought duration and severity in different seasons were also estimated. Additionally, Sen's slope values for the annual drought duration and severity at each station were estimated. To explore temporal and spatial patterns of drought characteristics, the average duration, severity, and their slopes during the past six decades were interpolated across the entire nation with 5-km spatial resolution using the inverse distance weight method. The temporal-spatial evolution of drought characteristics was further identified based on emerging hot spot analysis. Thirdly, annual drought duration and severity at the stations were aggregated to national and regional scales. Fourthly, EEMD was used to decompose the period characteristics and nonlinear trends. Finally, the relationships between drought disaster survey data and national and regional drought duration and severity estimates were examined.

3. Results

3.1. Spatial characteristics of drought

From the spatial distribution of mean drought duration over 1961–2020 (Fig. 4a), it can be seen that XJ, NM, western NE, NC, HH, northern QT, and western SW had larger mean drought duration than other regions, indicating that their regions had higher frequency of drought. The mean drought durations of the above-mentioned regions ranged from 105 to 267 days. Mean drought severity (Fig. 4b) showed a similar spatial distribution as observed for drought duration (Fig. 4a).

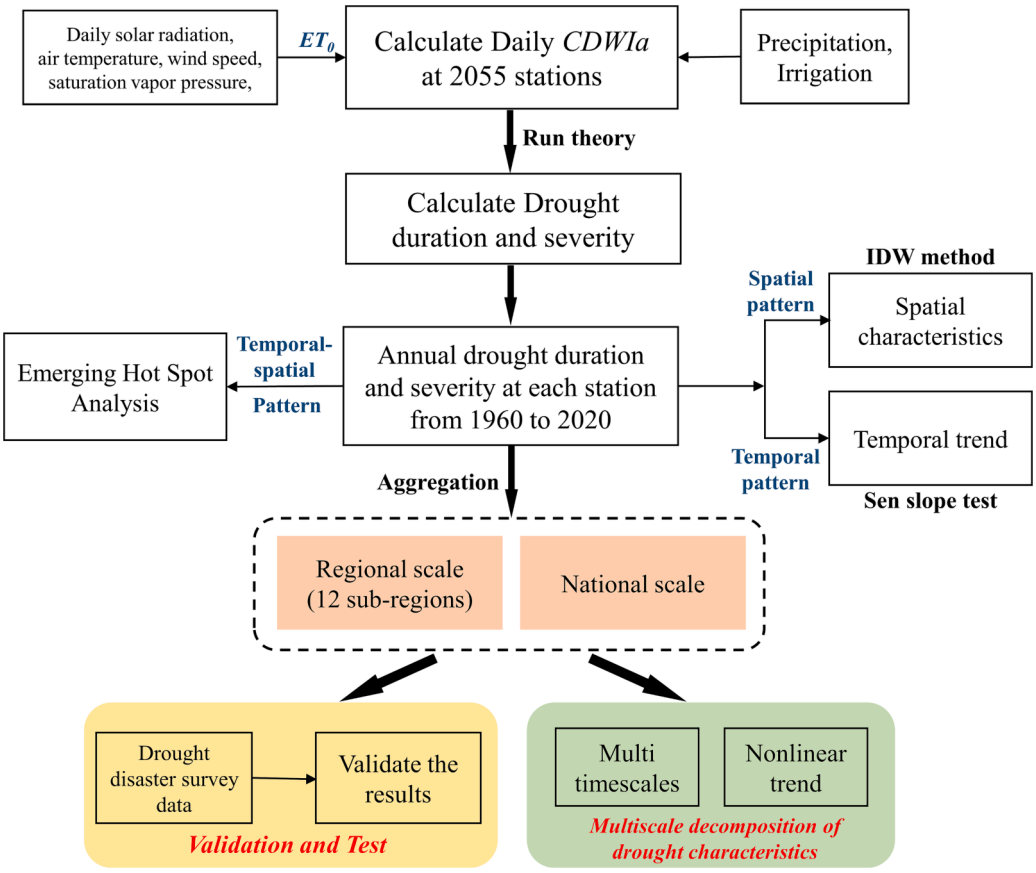

Fig. 3. Framework for drought analysis. Multiscale decomposition of drought characteristics is based on Ensemble Empirical Mode Decomposition. *CWDIa*: Crop Water Deficit Abnormal Index; IDW: inverse distance weight; ET_0: reference crop evapotranspiration.

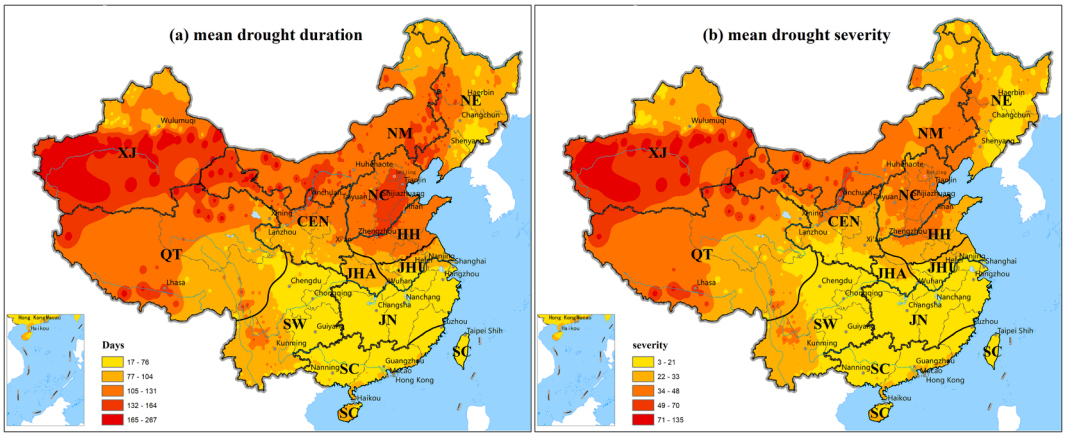

Fig. 4. Mean drought duration (a) and drought severity (b) from 1960 to 2020. NE: Northeast China; NC: North China; SC: South China; HH: Huanghuai district; JHA: Jianghan district; JHI: Jianghuai district; JN: Jiangnan district; NM: Inner Mongolia; QT: Tibetan Plateau region; CEN: East-central Northwest China; SW: Southwest China; XJ: Xinjiang.

The mean drought severity of the above-mentioned regions ranged from 34 to 135. JN, SC, and eastern SW had the lowest mean drought duration and lowest severity, ranging from 17 to 76 days and from 3 to 21, respectively.

Annual average drought days in the 12 regions are shown in Table 2. XJ had the greatest number of annual average drought days (150 days) and the greatest severity (57). The average drought duration for NC, HH, NM, and CEN was more than 100 days. SC and JN had fewer drought days (65 and 51 days, respectively) than other regions. JN had the smallest average drought severity.

The intra-annual distribution of average drought duration and severity in the 12 different regions varied (Table 2). There were more drought days or greater drought severity in winter and spring in NE, NC, HH, NM, QT, CEN, and SW. There was higher frequency in autumn and winter in SC, JHA, and JHU. Summer and autumn droughts were more obvious in JN.

In spring, drought duration values ranged from 26 to 76 days in western NE, NM, NC, northern CEN, and western of SW, which were more than in the other regions (Fig. 5a). JN and northern SC had the fewest average drought days (less than 15 days). In summer (Fig. 5b), the drought center was mainly located in northern and northwestern China, especially in XJ and NC. The mean drought duration ranged from 35 to 58 days. In autumn, eastern China and XJ had higher drought frequency than other regions, and drought duration was between 28 and 33 days (Fig. 5c). In winter, the mean drought duration in western NE, NM, XJ, CEN, NC, HH, QT, and western SW ranged from 30 to 73, and was larger than observed for the other regions. The spatial pattern of drought severity in different seasons (Fig. 6) was similar to the spatial pattern of drought duration (Fig. 5).

3.2. Temporal-spatial variations in drought characteristics

The temporal trends of agricultural drought characteristics (duration and severity) at each station estimated by Sen's Slope were interpolated over China (Fig. 7). In contrast to previously reported results from prior investigations, there was a discernible decline in both drought duration (Fig. 7a) and severity (Fig. 7b) across the majority of China. However, in contrast to this overarching trend, a notable increase in drought duration and severity was observed across most of SW, northern SC and JHA, southwestern NC, and western HH (Fig. 7). Table 3 and Table 4 provide a temporal summary of the decadal average and linear trend of drought characteristics, encompassing the entirety of China and 12 sub-regions. Specifically, the linear trend for drought duration (Table 3) and severity (Table 4) for China exhibited rates of −0.23 (days yr^{-1}) and −0.07 (days yr^{-1}), respectively, spanning the period from the 1960 s to the 2020 s.

The interdecadal variations in drought duration and severity underscores the distinct temporal trend (Table 3 and Table 4). Specifically, the temporal trends were characterized by a decline from the 1960 s to the 1980 s, followed by an increase from the 1980 s to the 1990 s, and then a renewed decrease spanning the 1990 s to the 2010 s. Paralleling the nationwide trend, a decreasing trend in drought duration was observed for most of the 12 regions, ranging between −0.03 and −0.91 (days yr^{-1}). Notably deviating from this pattern was an increase noted in JHA and SW (Table 3). Similarly, the prevailing trend in most regions,

Table 2
Seasonal and annual average drought duration (days) and severity from 1961 to 2020 in 12 regions.

Region	Drought duration (d)					Drought severity				
	Entire year	Spring	Summer	Autumn	Winter	Entire year	Spring	Summer	Autumn	Winter
NE	98	**33**	19	20	**26**	25	9	3	4	9
NC	135	**38**	25	28	**45**	41	11	5	7	18
SC	65	12	6	**23**	**23**	18	3	1	6	8
HH	119	**31**	23	27	**38**	33	8	5	7	13
JHA	93	18	22	**24**	**29**	21	3	4	6	8
JHI	84	15	17	**27**	**25**	19	3	3	7	7
JN	51	2	**13**	**27**	9	12	0	2	7	2
NM	135	**40**	25	29	**41**	41	13	5	7	16
QT	111	**32**	14	20	**45**	35	10	3	5	17
CEN	107	**27**	23	18	**39**	30	7	5	4	14
SW	71	**27**	9	7	**27**	17	7	2	1	7
XJ	150	**40**	35	**43**	32	57	16	10	16	15

NE: Northeast China; NC: North China; SC: South China; HH: Huanghuai district; JHA: Jianghan district; JHI: Jianghuai district; JN: Jiangnan district; NM: Inner Mongolia; QT: Tibetan Plateau region; CEN: East-central Northwest China; SW: Southwest China; XJ: Xinjiang.

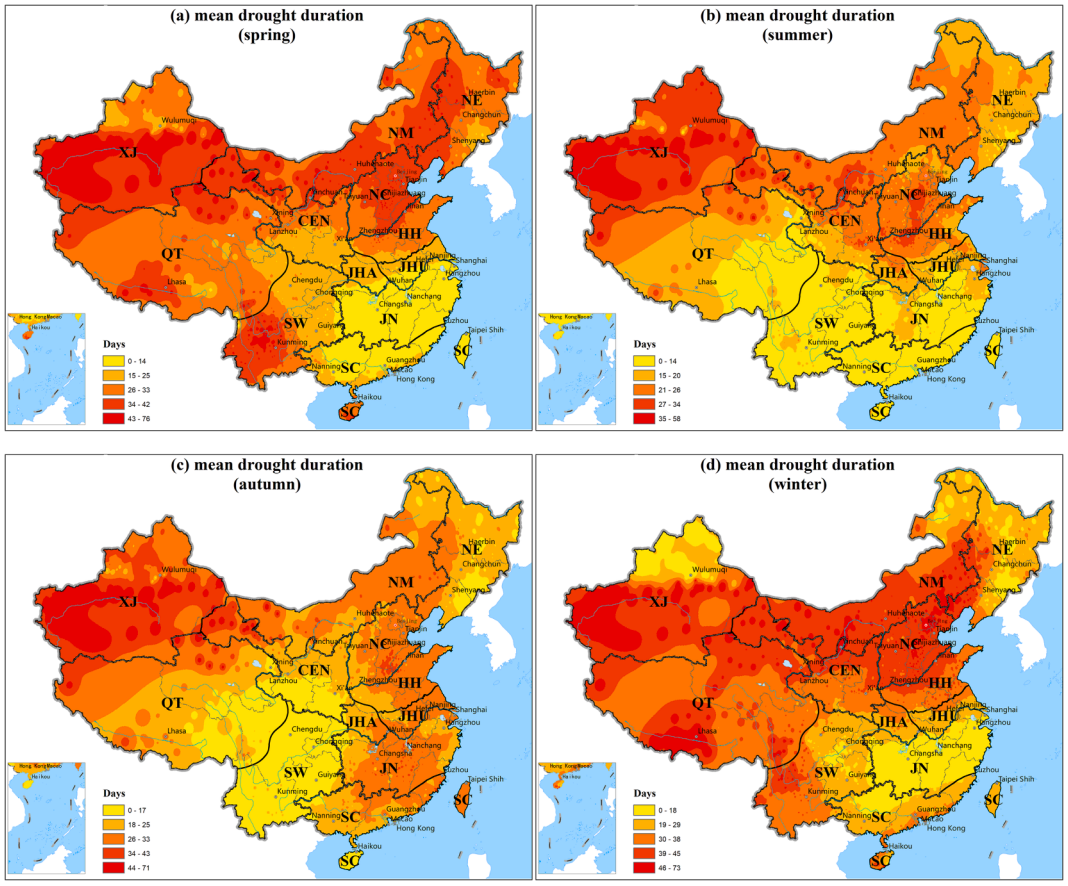

Fig. 5. Mean drought duration in spring (a), summer (b), autumn (c) and winter (d). NE: Northeast China; NC: North China; SC: South China; HH: Huanghuai district; JHA: Jianghan district; JHI: Jianghuai district; JN: Jiangnan district; NM: Inner Mongolia; QT: Tibetan Plateau region; CEN: East-central Northwest China; SW: Southwest China; XJ: Xinjiang.

except for SW, was a decline in drought severity (Table 4).

The interdecadal variation of drought duration exhibited four patterns (Table 3). For all of China, NE, SC, HH, JHU, and NM, the variation pattern was "Decrease-Increase-Decrease". NC and JHA had a "Decrease-Increase-Decrease-Increase" pattern. JN and CEN had an "Increase-Decrease-Increase-Decrease" pattern. QT and SW had a "Decrease-Increase" pattern. Similarly, the interdecadal variation of drought severity followed four patterns (Table 4). A "Decrease-Increase-Decrease" pattern appeared in China, NE, SC, HH, JHA, NM, and CEN. NC and JHU had a "Decrease-Increase-Decrease-Increase" pattern. JH had an "Increase-Decrease-Increase-Decrease" pattern. QT, SW, and XJ had a "Decrease-Increase" pattern.

Based on the sixteen patterns from the emerging spatiotemporal analysis, the study area was divided into multiple cold spot and hot spot regions (Fig. 8). Over the past six decades, variations in drought duration have highlighted hot spots (regions with higher duration, $P < 0.05$) in southern XJ and western QT. Furthermore, cold spots (regions with lower duration, $P < 0.05$) were found across southern China, the eastern Qinghai-Tibet Plateau, and the majority of northeastern China. These cold spot patterns were mainly identified as intensifying (4 %), persistent (9.4 %), sporadic (9.2 %), and oscillating (14.4 %). The spatial distribution of cold spots and hot spots for drought severity closely resembled that of drought duration, but with differences in temporal dynamics. Specifically, for drought severity, northeastern China and northern XJ displayed broader and stronger cooling trends, while persistent cold spot patterns dominated in southern China. Southern XJ and the western QT exhibited significant intensifying or persistent drying trends. The significant cold spots with oscillating pattern ($P < 0.05$) implied that these regions were previously identified as hot spots, while recent observations indicated a reduction in drought severity. If these trends persist, the drought conditions in these areas might be further alleviated in the future.

In summary, our analysis uncovered an overarching trend indicating the mitigation of agricultural drought across China. The amelioration of drought conditions enhanced the water supply to croplands, thereby increasing both crop yields and quality, ensuring the stability of farmers' livelihoods and the national food supply system. Furthermore, the decreases in drought helped to alleviate the pressures on soil degradation and water resource depletion, contributing to the preservation of ecosystem health and the sustainable development of the ecological environment.

3.3. *Multiscale decomposition of drought characteristics based on EEMD*

To explore the potential changes in long-term drought signals, we decomposed the interannual drought characteristics into different timescales using the EEMD method. The IMFs and trends were obtained from decomposing the time series of drought duration and severity (Figs. 9 and 10). For all of China, four modes were sufficient to decompose the complex dynamic signals. Specifically, the first and second modes represented inter-annual perturbations (quasi-3 and quasi-7-year for drought duration; quasi-3 and quasi-6 year for drought severity). And the third and fourth IMFs reflected inter-decadal cycle characteristics (quasi-15 and quasi-27 year for drought duration; quasi-12 and quasi-25 year for drought severity), which could be influenced by long-term atmospheric and oceanic factors (Table 5). The final component exhibited the slow-changing residual of climate oscillations, suggesting the intrinsic trend of the dataset (Table 5). In addition, the first

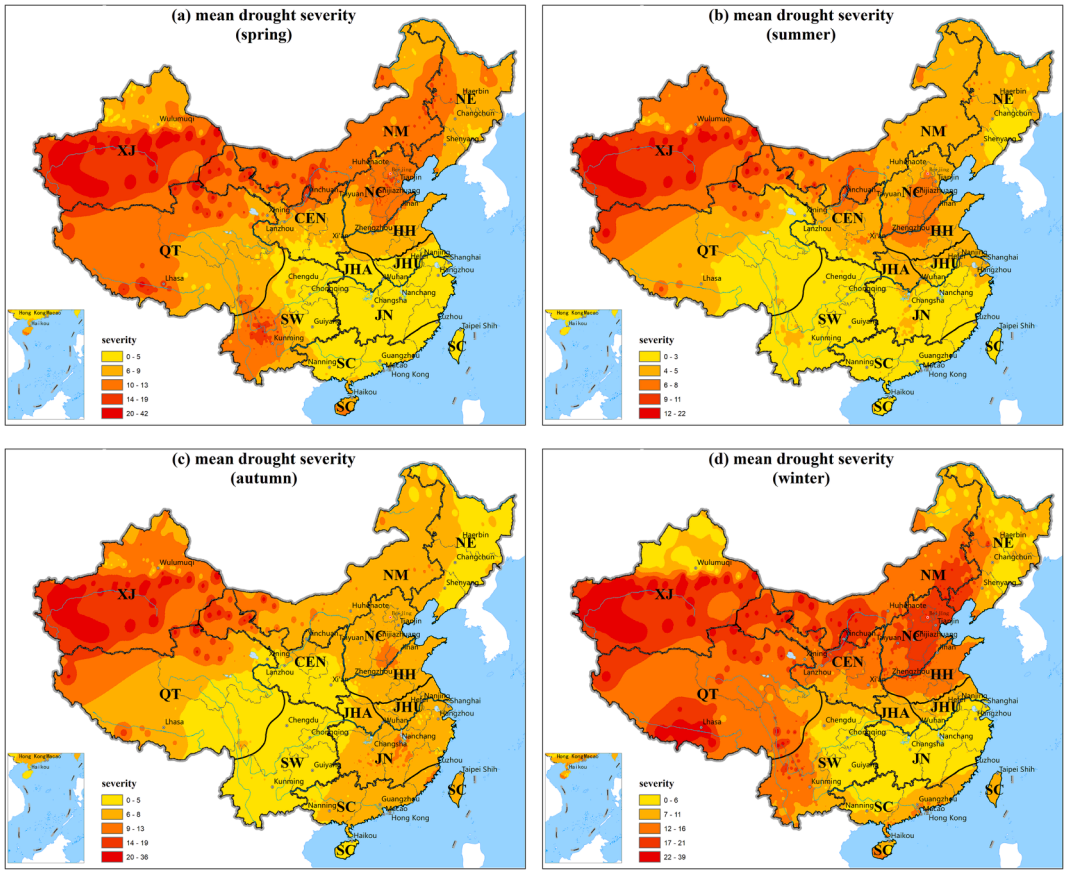

Fig. 6. Mean drought severity in spring (a), summer (b), autumn (c) and winter (d). NE: Northeast China; NC: North China; SC: South China; HH: Huanghuai district; JHA: Jianghan district; JHI: Jianghuai district; JN: Jiangnan district; NM: Inner Mongolia; QT: Tibetan Plateau region; CEN: East-central Northwest China; SW: Southwest China; XJ: Xinjiang.

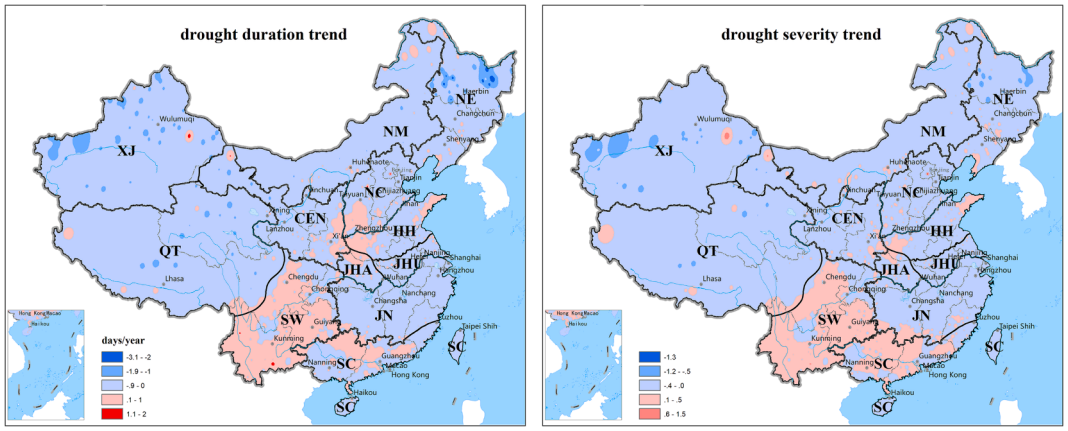

Fig. 7. Sen's slope of drought duration and severity from 1960 to 2020. NE: Northeast China; NC: North China; SC: South China; HH: Huanghuai district; JHA: Jianghan district; JHI: Jianghuai district; JN: Jiangnan district; NM: Inner Mongolia; QT: Tibetan Plateau region; CEN: East-central Northwest China; SW: Southwest China; XJ: Xinjiang.

IMF explained over 70 % of the variation in long-term drought characteristics, indicating that the nonlinear and non-stationary drought signal was mainly influenced by the inter-annual scale (Table 5). The mean drought duration and severity showed periodic variations, yet these fluctuations demonstrated a significant nonlinear decline over the last six decades (Figs. 9 and 10). Thus, the average drought characteristics in China were summarily characterized as periodic oscillations with a significant downward trend.

However, the trend of these drought characteristics varied among the 12 agricultural regions across China (Fig. 11). Drought duration showed an obvious downward trend in NE, QT, and XJ over the past 60 years. In addition, the time series of drought duration in SC, HHA, and SW exhibited a concave curve form with the inflection point appearing around the 1990 s. For NC, HHU, NM, and CEN, the trend of drought severity first increased and then decreased, with different mutation times (Fig. 11). Similar to the multi-scale decomposition at the national level, the IMF1 of the 12 regions explained the majority of the variations in drought duration (64.2 ± 7.7 % of the total variance, Table 6). The

Table 3
Decadal average drought duration (days) and Sen's slope trend rate for China and its 12 regions.

Region	1961–1970	1971–1980	1981–1990	1991–2000	2001–2010	2011–2020	Sen's slope (days/year)	Interdecadal variation pattern
China	103	97	91	94	92	88	−0.23	Decrease-Increase-Decrease
NE	118	105	89	101	91	86	−0.50	Decrease-Increase-Decrease
NC	140	133	139	149	124	128	−0.18	Decrease-Increase-Decrease-Increase
SC	74	61	62	64	74	55	−0.06	Decrease-Increase-Decrease
HH	132	110	122	123	113	118	−0.03	Decrease-Increase-Decrease
JHA	100	95	80	97	89	98	0.03	Decrease-Increase-Decrease-Increase
JHI	100	89	70	86	82	81	−0.25	Decrease-Increase-Decrease
JN	56	59	48	49	53	40	−0.22	Increase-Decrease-Increase-Decrease
NM	148	140	133	134	135	124	−0.25	Decrease-Increase-Decrease
QT	128	121	112	99	101	106	−0.53	Decrease-Increase
CEN	109	112	104	118	106	97	−0.28	Increase-Decrease-Increase-Decrease
SW	74	72	64	61	74	79	0.20	Decrease-Increase
XJ	180	169	151	141	129	136	−0.91	Decrease-Increase-Decrease-Increase

NE: Northeast China; NC: North China; SC: South China; HH: Huanghuai district; JHA: Jianghan district; JHI: Jianghuai district; JN: Jiangnan district; NM: Inner Mongolia; QT: Tibetan Plateau region; CEN: East-central Northwest China; SW: Southwest China; XJ: Xinjiang.

Table 4
Decadal average of drought severity and Sen's slope trend rate for China and its 12 regions.

Region	1961–1970	1971–1980	1981–1990	1991–2000	2001–2010	2011–2020	Sen's slope(/year)	Interdecadal variation pattern
China	30.1	26.9	24.9	26.6	24.9	24.4	−0.07	Decrease-Increase-Decrease
NE	34.1	25.0	21.7	25.0	22.0	22.9	−0.18	Decrease-Increase-Decrease
NC	44.3	40.4	40.5	46.3	35.5	37.9	−0.09	Decrease-Increase-Decrease-Increase
SC	20.6	16.8	16.4	17.8	21.6	14.2	−0.02	Decrease-Increase-Decrease
HH	37.3	29.9	32.6	35.3	30.5	30.8	−0.04	Decrease-Increase-Decrease
JHA	22.3	22.2	17.7	24.3	18.4	21.0	−0.01	Decrease-Increase-Decrease
JHI	22.8	22.3	15.4	20.9	17.0	18.2	−0.08	Decrease-Increase-Decrease-Increase
JN	12.8	14.4	10.3	11.1	12.4	9.3	−0.06	Increase-Decrease-Increase-Decrease
NM	47.2	41.7	39.5	40.8	40.2	38.9	−0.09	Decrease-Increase-Decrease
QT	41.9	38.3	34.2	30.3	30.8	35.3	−0.15	Decrease-Increase
CEN	32.3	29.7	29.9	34.3	28.4	26.2	−0.08	Decrease-Increase-Decrease
SW	18.9	17.0	15.1	13.9	18.4	19.2	0.05	Decrease-Increase
XJ	68.9	64.1	57.0	52.6	46.2	50.8	−0.38	Decrease-Increase

NE: Northeast China; NC: North China; SC: South China; HH: Huanghuai district; JHA: Jianghan district; JHI: Jianghuai district; JN: Jiangnan district; NM: Inner Mongolia; QT: Tibetan Plateau region; CEN: East-central Northwest China; SW: Southwest China; XJ: Xinjiang.

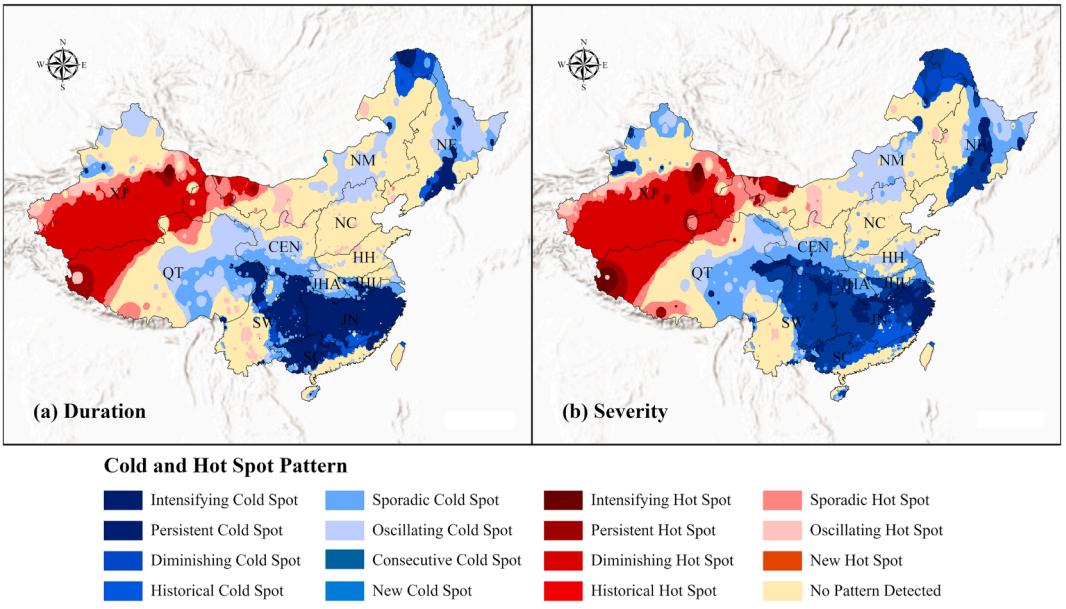

Fig. 8. Emerging Hot Spot Analysis to identify temporal-spatial cluster trends of drought characteristics. Various patterns of cold spots and hot spots are shown in blue and red, respectively. NE: Northeast China; NC: North China; SC: South China; HH: Huanghuai district; JHA: Jianghan district; JHI: Jianghuai district; JN: Jiangnan district; NM: Inner Mongolia; QT: Tibetan Plateau region; CEN: East-central Northwest China; SW: Southwest China; XJ: Xinjiang. (For interpretation of the references to colour in this figure legend, the reader is referred to the web version of this article.)

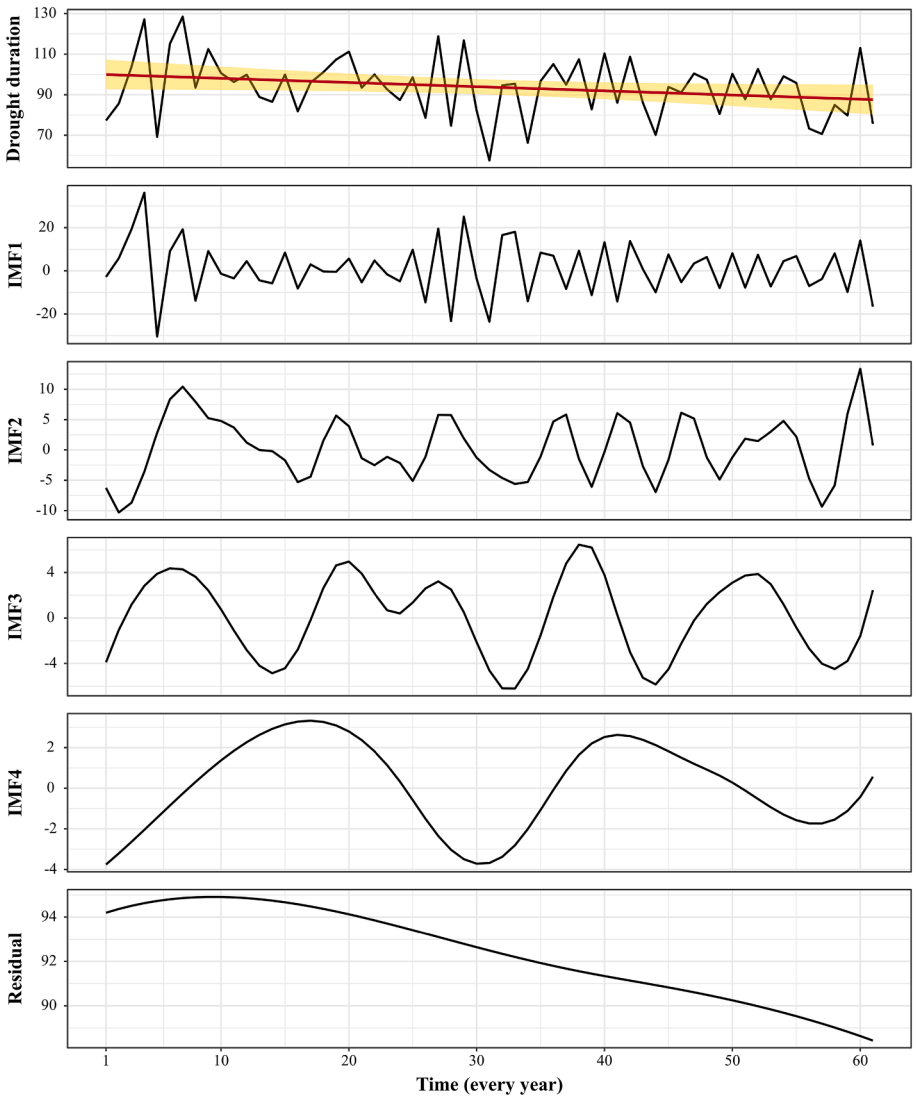

Fig. 9. Original signal of drought duration decomposed into four intrinsic mode function (IMF) components and a residual by Ensemble Empirical Mode Decomposition. The yellow band and red line in the top panel represent the 95% confidence interval and the linear trend for the original signal, respectively. (For interpretation of the references to colour in this figure legend, the reader is referred to the web version of this article.)

contributions of the second, third, and fourth modes decreased sequentially, with IMF2 accounting for 17.3 ± 7.1 %, IMF3 accounting for 10.0 ± 3.5 %, and IMF4 accounting for 3.6 ± 3.2 % of the variations. It is noteworthy that the variance contribution and period of the fourth mode in QT were significantly higher than in the other regions (13.2 % and 40-year, respectively), indicating that the inter-decadal scale influenced by long-term atmospheric factors is an important periodic characteristic (Table 6).

In most regions, the temporal patterns for long-term drought severity were similar to those for drought duration (Fig. 11). Specifically, we observed a significant downward trend in NE, HH, NM, QT, and CEN, and a concave curve in SC and SW. In contrast, HH, long-term drought severity showed the opposite pattern, with more persistent but milder droughts (Fig. 11). In addition, we also found that the variance contribution and period of the fourth mode of drought severity (9 % and 42-year, respectively) in QT deviated significantly from the mean level (Table 7). This highlighted the fact that the drought characteristics on the Qinghai-Tibet Plateau were regulated not only by interannual weather conditions but also by long-term climate warming and oceanic patterns. In general, drought duration and severity showed similar frequency changes, but there were significant differences in the long-term drought characteristics among the different regions.

3.4. Detecting actual drought disaster

To validate the effectiveness and practicality of the drought index proposed in this study for detecting actual drought coverage and affected areas, we conducted statistical verification and provided high-precision correlation based on officially released field survey data on drought (Fig. 12). The drought duration derived from *CWDIa* captured about 80 % of the variations in drought-covered and drought-affected areas (with R^2 of 0.85 and 0.78, respectively, and $P < 0.001$). For each additional 10 days of drought duration, there was a corresponding 1.54 % increase in the drought-covered area and a 0.71 % increase in the drought-affected area (Fig. 12a and b). Notably, the impact of increased drought severity on drought disasters was more than three times greater than that of increased drought duration. The significant relationship between drought severity and drought-covered/affected area was confirmed in Fig. 12 (with R^2 of 0.84 for drought-covered area and R^2 of 0.76 for drought-affected area). Specifically, for each increase of 10 in drought severity, the drought-covered and drought-affected areas increased by 5.4 % and 2.5 %, respectively.

The boundaries of each climatic zone do not entirely coincide with provincial borders. As a result, we extracted drought disaster statistics from the main provinces within each sub-region to validate the drought

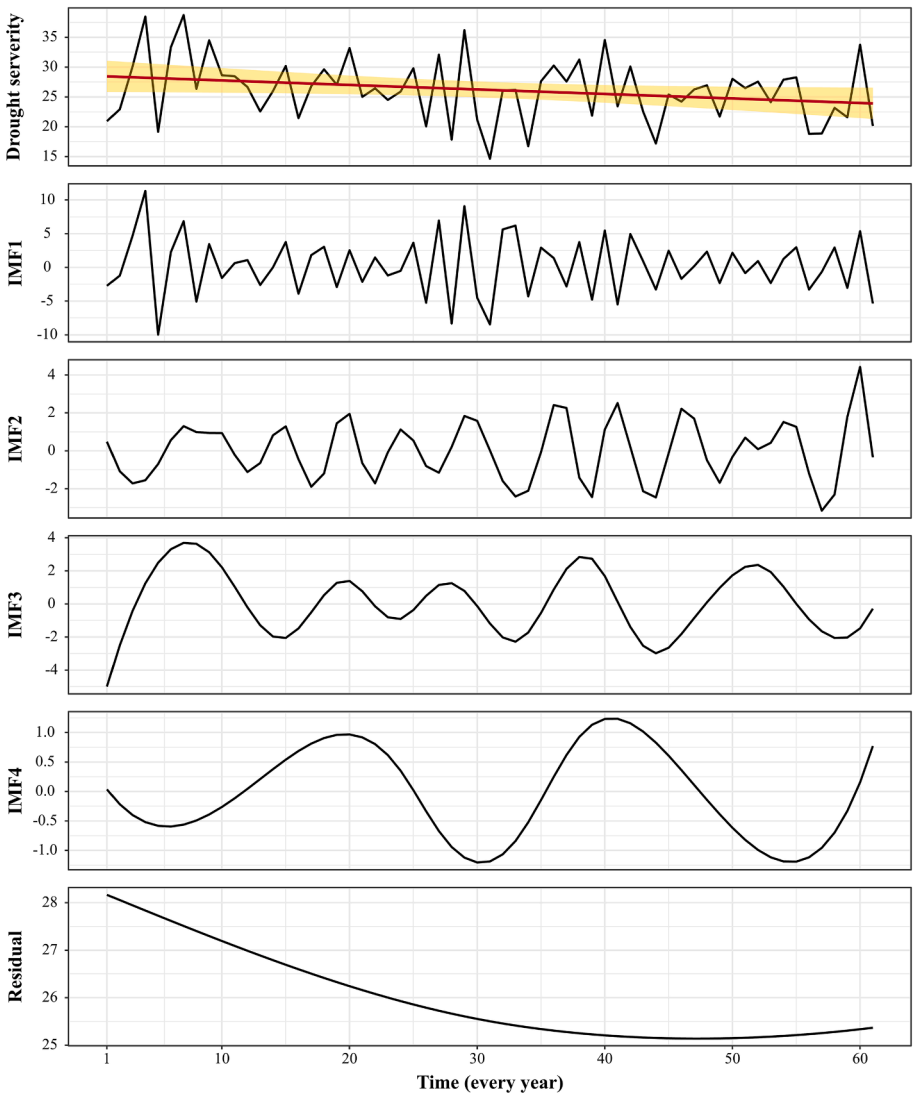

Fig. 10. Original signal of drought severity decomposed into four intrinsic mode function (IMF) components and a residual by Ensemble Empirical Mode Decomposition. The yellow band and red line in the top panel represent the 95% confidence interval and the linear trend for the original signal, respectively. (For interpretation of the references to colour in this figure legend, the reader is referred to the web version of this article.)

Table 5
The period and variance contribution of IMFs and trend for national drought duration and severity.

		IMF1	IMF2	IMF3	IMF4	Trend
Drought duration	Period (years)	2.6	7.1	14.5	26.5	–
	Variance contribution (%)	76.2	13.5	5.8	1.9	2.5
Drought severity	Period (years)	2.6	6	11.6	24.5	–
	Variance contribution (%)	72.8	9.2	12.1	2.1	3.8

monitoring performance of *CWDIa*. We found a robust linear relationship between drought duration and the drought-covered area with R^2 values ranging from 0.57 to 0.77 (Fig. S1). Upon implementing drought duration onto the drought-affected area, a slight decrease in effectiveness was observed ($R^2 = 0.42–0.69$, Fig. S2). Similarly, drought severity also effectively captured the covered area (R^2 values ranging from 0.56 to 0.75, Fig. S3) and the affected area (R^2 values ranging from 0.44 to 0.69, Fig. S4) within each sub-region. Overall, the drought index developed in this study robustly and accurately reflected actual drought occurrence, and therefore has significant implications and potential applications for guiding drought management.

4. Discussion

4.1. Performance of multiple drought indices in assessing drought disaster

The results of this study, based on agricultural drought statistics, provided compelling evidence for the effectiveness of a drought monitoring framework using the *CWDIa* method and a dense network of observations. Our findings demonstrated the exceptional performance of the framework in accurately detecting drought events and precisely capturing drought-covered and drought-affected areas across China (Fig. 12). Our method outperformed commonly used drought indices, with R^2 values exceeding 0.8. For example, Cai et al. (2023) found that the multisource remote sensing-derived Scaled Drought Condition Index explained only 35 % of the drought area derived from statistical data. Moreover, Zhang et al. (2023) introduced the Crop Water Anomaly Percentage Index that considered crop water demand, and achieved a higher correlation coefficient of 0.79 with the simulated drought area, outperforming the Soil Moisture Anomaly Percentage Index. This remarkable drought assessment performance can be attributed to the extensive coverage provided by over 2000 observation sites throughout

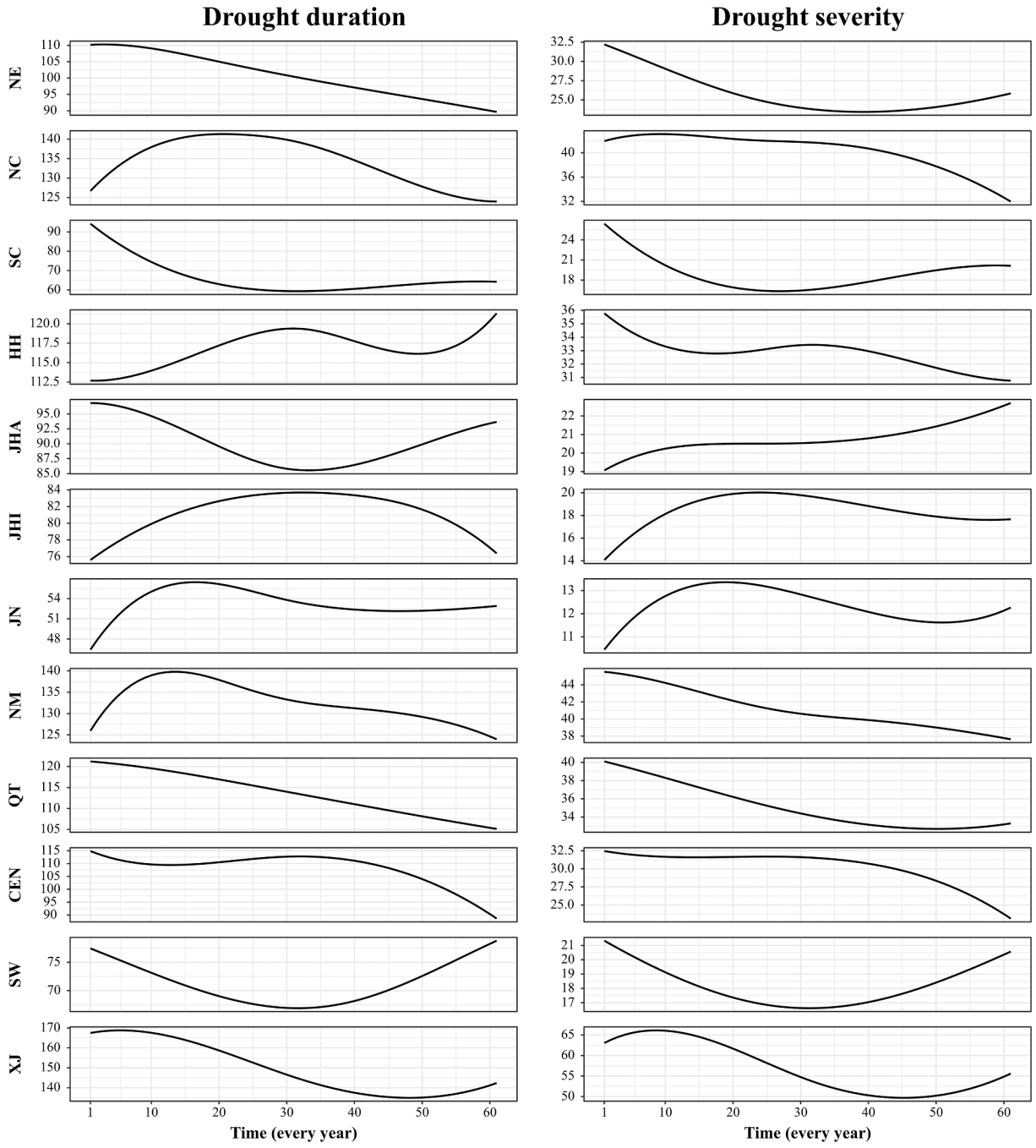

Fig. 11. Residuals of drought duration and severity decomposed by Ensemble Empirical Mode Decomposition in different regions. NE: Northeast China; NC: North China; SC: South China; HH: Huanghuai district; JHA: Jianghan district; JHI: Jianghuai district; JN: Jiangnan district; NM: Inner Mongolia; QT: Tibetan Plateau region; CEN: East-central Northwest China; SW: Southwest China; XJ: Xinjiang.

China.

Incorporation of site-based observational drought indices in this study effectively avoided the uncertainties arising from remote sensing products, including sensor errors and atmospheric disturbances. Previous investigations focusing on site-based analyses have successfully attained multiscale drought estimations across China. Wang et al. (2021) constructed an extensive daily dataset of SPEI using data from 427 observation stations across mainland China, spanning the period from 1961 to 2018. Furthermore, Wu et al. (2020) conducted a comprehensive analysis of China's drought characteristics over the past 60 years by integrating monthly meteorological data from 618 stations nationwide and the Penman-Monteith equation. Nonetheless, these studies were constrained by their reliance on a limited number of observations that hindered the acquisition of reasonable spatiotemporal patterns and unbiased estimates of drought characteristics. The inherent uncertainty from data sparsity in certain regions is a substantial challenge for monitoring drought. Hence, a crucial contribution of this study is the provision of more precise, continuous, and multiscale estimates of drought characteristics that comes from utilizing a network of over two thousand long-term observation sites.

In addition, the drought indices used in this study considered climate characteristics and crop water demand to assess agricultural drought. In previous investigations, soil moisture has frequently been adopted as a proxy for the water balance to depict agricultural drought, embodying the interaction among precipitation, evapotranspiration, groundwater, and irrigation practices. Nevertheless, the incorporation of soil moisture

Table 6
The period and variance contribution of IMFs and trend for regional drought duration.

Region	IMF1		IMF2		IMF3		IMF4		Trend	
	Period (years)	Variance contribution (%)	Period (years)	Variance contribution (%)	Period (years)	Variance contribution (%)	Period (years)	Variance contribution (%)	Period (years)	Variance contribution (%)
NE	2.9	67.8	6.2	11.9	18.0	12.5	35.3	2.5	–	5.3
NC	3.0	70.3	6.0	14.1	16.0	11.6	16.7	0.8	–	3.2
SC	2.8	61.9	5.7	5.0	14.0	15.0	55.0	4.7	–	13.5
HH	2.7	79.1	5.8	9.9	11.8	9.9	20.0	0.6	–	0.5
JHA	2.5	65.3	5.6	15.1	12.2	13.6	25.3	4.6	–	1.3
JHI	2.9	62.3	7.0	27.5	13.8	5.4	32.7	4.3	–	0.5
JN	2.8	62.5	6.1	18.9	13.4	15.3	20.8	2.0	–	1.3
NM	2.5	64.4	6.3	22.7	11.2	7.4	28.5	2.7	–	2.8
QT	3.4	57.1	10.2	16.1	16.0	4.5	40.0	13.2	–	9.1
CEN	3.4	73.4	6.8	13.6	13.8	8.4	25.0	1.1	–	3.5
SW	2.9	57.1	6.5	30.0	11.8	7.5	33.0	3.2	–	2.2
XJ	2.7	48.9	6.6	23.3	11.6	8.3	28.0	3.6	–	15.9

NE: Northeast China; NC: North China; SC: South China; HH: Huanghuai district; JHA: Jianghan district; JHI: Jianghuai district; JN: Jiangnan district; NM: Inner Mongolia; QT: Tibetan Plateau region; CEN: East-central Northwest China; SW: Southwest China; XJ: Xinjiang.

Table 7
The period and variance contribution of IMFs and trend for regional drought severity.

Region	IMF1		IMF2		IMF3		IMF4		Trend	
	Period (years)	Variance contribution (%)	Period (years)	Variance contribution (%)	Period (years)	Variance contribution (%)	Period (years)	Variance contribution (%)	Period (years)	Variance contribution (%)
NE	2.7	64.2	6.2	13.3	18.3	10.3	36.0	4.2	–	8.0
NC	2.8	70.3	5.3	12.7	12.0	12.3	18.4	0.4	–	4.3
SC	2.7	65.5	8.6	10.9	11.8	13.8	27.5	2.1	–	7.7
HH	2.9	74.7	5.5	10.6	11.8	12.7	20.4	0.8	–	1.2
JHA	2.5	67.0	5.6	13.4	12.2	16.6	27.5	2.4	–	0.7
JHI	2.8	69.3	5.9	15.2	12.2	8.5	27.5	5.6	–	1.4
JN	3.0	61.4	6.7	17.3	14.3	18.8	28.0	1.6	–	0.9
NM	2.5	67.2	5.4	21.0	12.4	5.3	22.4	3.0	–	3.4
QT	3.2	47.2	8.6	31.6	18.3	3.9	42.0	9.0	–	8.2
CEN	2.9	61.8	7.6	16.4	15.4	15.5	55.0	1.2	–	5.2
SW	3.0	64.9	6.7	19.1	12.4	8.6	37.3	2.5	–	4.9
XJ	2.9	48.5	6.6	18.9	11.6	9.1	28.5	2.1	–	21.3

NE: Northeast China; NC: North China; SC: South China; HH: Huanghuai district; JHA: Jianghan district; JHI: Jianghuai district; JN: Jiangnan district; NM: Inner Mongolia; QT: Tibetan Plateau region; CEN: East-central Northwest China; SW: Southwest China; XJ: Xinjiang.

measurements in long-term site observations is a costly and scarce option. Additionally, currently available spatiotemporally continuous soil moisture datasets, such as GLDAS, FLDAS, ERA5-Land, and MERRA-2, unavoidably introduce substantial errors and uncertainties due to incomplete consideration of water balance processes, systematic errors in modeling, challenges in characterizing human management practices, limited in-situ observations, and coarse spatiotemporal resolutions (Zeng et al., 2015; Zhang et al., 2017; Chen et al., 2020). Previous investigations have revealed considerable disparities in assessing agricultural drought in China through the utilization of model-simulated and satellite-derived soil moisture data. Our study not only highlighted the importance of integrating climate characteristics and crop water demand into drought indices for agricultural drought assessment, but also provided a practical alternative framework as a replacement for predicted soil moisture data.

4.2. *Spatiotemporal patterns of drought characteristics in China*

Our findings indicated that average drought duration and severity over the past sixty years in China exhibited similar geographic patterns (Fig. 4). Specifically, drought severity was more pronounced in the northwestern and northern regions of China (including the North China Plain and Inner Mongolia grassland-desert belt), while the southern regions experienced relatively milder drought conditions. Yang et al. (2023) also observed more severe drought using the multivariate drought index on the Qinghai-Tibet Plateau and the North China Plain compared with the southern regions, exhibiting consistent spatial patterns of drought duration and severity with our study. Furthermore, severe drought conditions were also observed in the northern regions of Yunnan (Fig. 4), a finding that is corroborated by other studies (Lin et al., 2015; Zhao et al., 2023). In recent years, decreased precipitation in southwestern China has triggered severe drought, resulting in the spread of meteorological drought to agricultural drought (Yu et al., 2019). The drought monitoring framework introduced in this study effectively captured the spatial evolution of drought.

In addition, our findings indicated a progressive mitigation of drought in most regions of China during 1960 to 2020 except in southwestern China (including Yunnan, Guizhou, Guangxi, and Guangdong) (Fig. 7). The high temperatures and persistent decrease in precipitation induced by atmospheric circulation anomalies were the primary drivers of drought in the southwestern region (Zhang et al., 2012; Zhang et al., 2013). More than 50 % of water deficits occurred from September to March of the following year (Figs. 5 and 6), resulting in significant water shortages (Yu et al., 2019). These findings have been robustly supported by previous studies (Zhang et al., 2012). He et al. (2023) employed a coupled SPI dataset incorporating meteorological station data and topographic data over the past forty years and found temporal drought trend characteristics that were consistent with the results of our study. They observed a decreasing trend in both severity and duration of drought in China at seasonal and annual scales, particularly in the northwestern region and the Tibetan Plateau (He et al., 2023). However, in Northeast China, the SPI-based estimates exhibited a stronger drying trend, possibly because SPI focuses on meteorological drought rather than considering crop water demand.

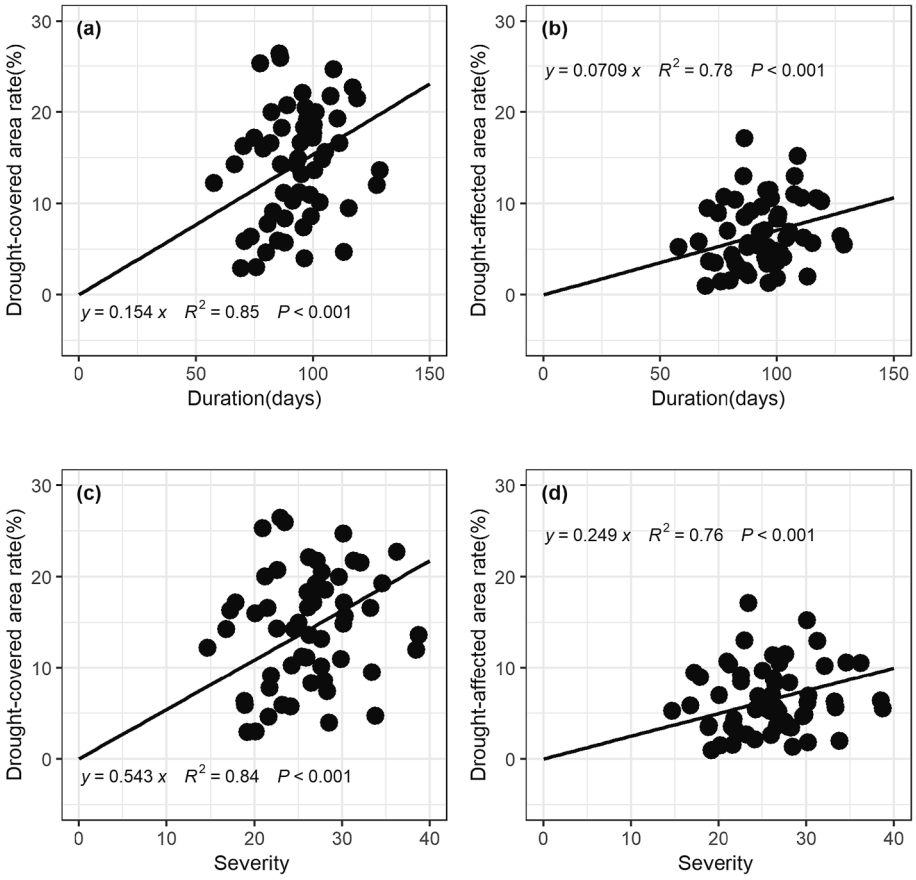

Fig. 12. Relationships between drought characteristics and actual drought-covered area rate (**a** and **c**) and drought-affected area rate (**b** and **d**).

The multiscale decomposition of drought characteristics further strengthened the temporal pattern identified in this study because it was able to separate the long-term trends from the complex drought signals having periodicity (Figs. 9, 10, and 11). Specifically, (1) Overall drought conditions in China have lessened over the past 60 years, and the northwest region has exhibited a warm and moist trend (Peng and Zhou, 2017) ; (2) Droughts have intensified in the North China Plain and southwestern region (Zhang et al., 2019; He et al., 2023); and (3) Droughts have decreased on the Tibetan Plateau (He et al., 2023). The application of EEMD for decomposing drought characteristics provided more robust and precise trend estimations, avoiding the interference caused by cross-scale periodic signals.

4.3. Potential attribution for overall drought alleviation

This study revealed an overall alleviation of agricultural drought in China across spatiotemporal scales based on observations from 2000 monitoring sites. However, intensified drought conditions persisted in specific regions (Fig. 7, Table 3, and Table 4). These findings are consistent with previous studies based on site-level observations, gridded data, and modeling (Wang et al., 2017b; Zeng et al., 2020; He et al., 2023). Drought assessment based on drought indices relies on the dynamic interplay between water supply (precipitation) and water demand (actual evapotranspiration). Most of the observation sites located in drought-alleviated regions experienced a range of temperature increases (Tmax, Tmin, and Tmean), along with augmented precipitation and decreased ET_0 (Yao et al., 2018; Pan et al., 2023). While the sustained rise in temperature exacerbates evapotranspiration to drive the evolution of drought, the compensation effect of increased precipitation might generate more positive contributions within intricate hydrological processes, potentially leading to an overall alleviation of drought conditions (Feng et al., 2023). The influence of dynamic interplay between precipitation and evapotranspiration on drought patterns has been investigated in past research. Most of those studies have posited that lack of precipitation stands as the primary driver for the evolution of drought in northern regions, whereas evapotranspiration (ET) plays a more prominent role in driving drought changes in southern areas (Liu et al., 2022; Guo et al., 2023; Wan et al., 2023). The reduction in drought severity and duration in northern regions corresponds to an increasing trend in precipitation, especially evident in the northwest. This implies that increased precipitation in northern China has alleviated drought and reduced agricultural drought risk (Guo et al., 2023). The abundant water supply in southern and southwestern China has the potential to meet the atmospheric evaporation requirements and to support vegetation physiological activities, exacerbating agricultural drought (Wang et al., 2022; Guo et al., 2023).

The variations in precipitation and ET can be further explained by the large-scale atmospheric circulation characteristics, sea surface temperature anomalies, and anthropogenic activities(Jin et al., 2013; Horton et al., 2015). For instance, the El Niño-Southern Oscillation serves as a pivotal driving factor for changes in precipitation and temperature across tropical and temperate regions, exerting varying degrees of impact on the climatic conditions of different sub-regions in China (Hao et al., 2018). The El Niño occurring in the tropical Pacific Ocean can potentially weaken the Northwestern Pacific Subtropical High and the East Asian summer monsoon, resulting in insufficient moisture transport to China and ultimately causing drought. Conversely, La Niña weakens the transport capacity of the Southeast and Southwest moisture channels, directly leading to drought (Wang et al., 2017a). Furthermore, Guo et al. (2023) found that the Atlantic Multidecadal Oscillation exacerbated the severity of drought in the Yangtze River Basin and the Pearl River Basin. Additionally, the North Atlantic Oscillation exhibited

an ascending trend, particularly concentrated in the southern regions, thereby contributing dynamically to prolonged drought duration. Human activities (such as land use changes, irrigation, and reservoir management) can either promote or suppress drought propagation by altering the hydrological cycle (Zhou et al., 2019). For instance, a range of ecological engineering practices implemented in China in the 21st century, such as water diversion, desertification control, and afforestation, has enhanced soil water retention. This subsequently has increased precipitation and relative humidity, indirectly alleviating agricultural drought (Wang et al., 2017b; Pan et al., 2023). In summary, the overall alleviation of drought in China has been due to the combined influence of climate and human activities. The attribution of changes in drought characteristics in specific regions necessitates context-dependent analyses.

4.4. Limitations and perspectives

Despite these findings, our study had some limitations that need to be further clarified. Firstly, although *CWDIa* considers various climatic factors affecting crop water balance and maintains a high level of consistency with prior studies in nationwide agricultural drought assessment, its calculations predominantly focused on crop water requirements. As a consequence, careful consideration is necessary when extrapolating its application beyond agricultural contexts. Specifically, China's heterogeneous and vast geographical expanse encompasses a range of diverse underlying environments such as forests, grasslands, and deserts. Applying *CWDIa* based on crop coefficients and reference crop evapotranspiration can potentially underestimate actual water depletion in desert or barren terrains. And its application in forests or grasslands could also lead to some degree of overestimation or underestimation, depending on geographical distribution, climate conditions, and vegetation types. In non-agricultural settings, direct application of *CWDIa* without prior coefficient calibration or site validation will likely introduce certain limitations for drought estimation. Therefore, we emphasize prioritizing the application of *CWDIa* for assessing agricultural drought. Next, our study incorporated the most comprehensive observation network, but the lack of stations on the Tibetan Plateau and in Xinjiang remains a notable limitation, potentially introducing uncertainties in regional drought assessment. While estimates of drought characteristics in Xinjiang and on the Tibetan Plateau have been corroborated by other studies, the quantification of uncertainties in these estimations remains challenging. Future studies may overcome this limitation by use of data assimilation techniques that integrate observations and remote sensing data.

In addition, the absence of irrigation components in the drought indices can introduce uncertainty in the detection of agricultural drought, particularly in irrigated regions (Zhang et al., 2023). Irrigation practices increase soil moisture and mitigate the photosynthetic limitations caused by dry-hot climates, thereby restricting the spread of meteorological drought into agricultural drought. However, not all regions in China require irrigation to compensate for water deficits; for instance, sufficient precipitation and the high cost of irrigation in southern China mitigate the necessity for irrigation. Actual irrigation rates for agricultural activities remain at low levels even in arid regions (national average irrigation rate in 2019 = 6.8 ± 15.7 %; average irrigation rate in cropland = 19.5 ± 21.3 %, Fig. S5). Furthermore, obtaining comprehensive site-specific irrigation statistics remains challenging in practice. Actual irrigated quotas and areas in current irrigation maps may be significantly underestimated compared with statistical data due to crop rotation, water scarcity, and damage to irrigation infrastructure. Despite this, the actual application of *CWDIa* was not hindered. Regions with available irrigation statistics can integrate them as inputs, while *CWDIa* without irrigation data can still provide accurate nationwide estimates. In the future, developing precise and dynamic irrigation maps and incorporating irrigation timing and quotas based on publicly available and comprehensive statistics will be a critical challenge in evaluating drought disasters using drought indices.

This study provided a multidimensional assessment of agricultural drought based on *CWDIa* that considered meteorological factors and crop water requirements. This approach facilitated the design of prioritized and differentiated policy attention and regional resource allocations towards various agricultural drought hot spots. The identification of spatiotemporal variations, sensitivity, and potential future evolutions in drought characteristics demonstrates the distribution of agricultural drought risks at varying confidence levels. Incorporating such assessments into national or regional disaster management and prevention strategies would be beneficial for gradually mitigating the impacts of drought. As climate change continues to amplify the risk of drought, there is a pressing need to further conduct research on drought hazards, develop drought early warning systems, and enhance drought mitigation strategies in high-risk regions (Khoshnazar et al., 2023). In summary, our study established a comprehensive and dependable framework for assessing agricultural drought in China, thereby promoting the transition from hazard assessment to risk evaluation in the context of providing reliable information for future research directions.

5. Conclusions

We integrated data from 2055 stations and *CWDIa* to quantify the spatiotemporal variations of agricultural drought characteristics in China over the past 60 years. EEMD was used to effectively separate complex drought signals into their multiscale periodic variations. The results indicated that the duration and severity of drought in northern China were significantly higher than in the southern regions, particularly in the northwestern part, the North China Plain, and the northern Tibetan Plateau. Persistent water deficits during the spring and winter seasons in the southwestern regions and the southern Tibetan Plateau drove the occurrence of more severe droughts. Over the past 60 years, agricultural drought severity and duration have generally decreased in China, but an increasing drought trend was observed in southwestern China and parts of the North China Plain based on EEMD. The integration of *CWDIa* and a dense network of in-situ observations in the drought monitoring framework robustly captured about 80 % of the actual drought-covered and drought-affected areas. Our findings provided compelling evidence for assessing the spatiotemporal patterns of drought characteristics over the past 60 years using extensive observations across China. The study results underscored the significance of incorporating multiple climatic factors and crop water demand into the drought assessment. Accurate drought estimates will contribute to governments and stakeholders being able to make timely adjustments to agricultural policies and to implement adaptations in order to mitigate crop yield failure.

CRediT authorship contribution statement

Ning Jin: Methodology, Formal analysis, Writing – original draft, Writing – review & editing, Software. **Yu Shi:** Conceptualization, Methodology, Formal analysis, Writing – original draft, Writing – review & editing, Software. **Wenhao Niu:** Validation, Writing – review & editing. **Liang He:** Conceptualization, Methodology, Software, Data curation.

Declaration of competing interest

The authors declare that they have no known competing financial interests or personal relationships that could have appeared to influence the work reported in this paper.

Data availability

Data will be made available on request.

Acknowledgements

This work was funded by the Science and Technology Innovation 2030—" New Generation Artificial Intelligence" Major Project (2021ZD0113605). Ning Jin acknowledges the support of the General Program of Natural Science Research, Fundamental Research Program of Shanxi Province (202203021221231).

Appendix A. Supplementary data

Supplementary data to this article can be found online at https://doi.org/10.1016/j.jhydrol.2023.130454.

References

AghaKouchak, A., 2014. A baseline probabilistic drought forecasting framework using standardized soil moisture index: application to the 2012 United States drought. Hydrol. Earth Syst. Sci. 18, 2485–2492. https://doi.org/10.5194/hess-18-2485-2014.

Allen, R.G., Pereira, L.S., Raes, D., Smith, M., 1998. Crop evapotranspiration-Guidelines for computing crop water requirements-FAO Irrigation and drainage paper 56. Fao, Rome. 300, D05109.

Cai, S., Zuo, D., Wang, H., Xu, Z., Wang, G., Yang, H., 2023. Assessment of agricultural drought based on multi-source remote sensing data in a major grain producing area of Northwest China. Agric. Water Manage. 278, 108142 https://doi.org/10.1016/j.agwat.2023.108142.

Chen, N., Li, R., Zhang, X., Yang, C., Wang, X., Zeng, L., Tang, S., Wang, W., Li, D., Niyogi, D., 2020. Drought propagation in Northern China Plain: A comparative analysis of GLDAS and MERRA-2 datasets. J. Hydrol. 588, 125026 https://doi.org/10.1016/j.jhydrol.2020.125026.

China Meteorological Administration, 2015. Grade of Agricultural Drought. Standards Press, Beijing, China in Chinese.

China Meteorological Administration, 2018. Geographical partition of meteorlolgical products in China. Standards Press, Beijing, China in Chinese.

Clarke, D., Hess, T.M., Haro-Monteagudo, D., Semenov, M.A., Knox, J.W., 2021. Assessing future drought risks and wheat yield losses in England. Agric. for. Meteorol. 297, 108248 https://doi.org/10.1016/j.agrformet.2020.108248.

Dai, A., 2011. Drought under global warming: a review. Wiley Interdiscip. Rev.-Clim. Chang. 2, 45–65. https://doi.org/10.1002/wcc.81.

Feng, K., Yan, Z., Li, Y., Wang, F., Zhang, Z., Su, X., Wu, H., Zhang, G., Wang, Y., 2023. Spatio-temporal dynamic evaluation of agricultural drought based on a three-dimensional identification method in Northwest China. Agric. Water Manage. 284, 108325 https://doi.org/10.1016/j.agwat.2023.108325.

Guo, W., Huang, S., Huang, Q., She, D., Shi, H., Leng, G., Li, J., Cheng, L., Gao, Y., Peng, J., 2023. Precipitation and vegetation transpiration variations dominate the dynamics of agricultural drought characteristics in China. Sci. Total Environ. 898, 165480 https://doi.org/10.1016/j.scitotenv.2023.165480.

Han, X., Wu, J., Zhou, H., Liu, L., Yang, J., Shen, Q., Wu, J., 2020. Intensification of historical drought over China based on a multi-model drought index. Int. J. Climatol. 40, 5407–5419. https://doi.org/10.1002/joc.6527.

Hao, Z., Singh, V.P., Xia, Y., 2018. Seasonal Drought Prediction: Advances, Challenges, and Future Prospects. Rev. Geophys. 56, 108–141. https://doi.org/10.1002/2016RG000549.

He, Q., Wang, M., Liu, K., Li, B., Jiang, Z., 2023. Spatiotemporal analysis of meteorological drought across China based on the high-spatial-resolution multiscale SPI generated by machine learning. Weather Clim. Extremes. 40, 100567 https://doi.org/10.1016/j.wace.2023.100567.

Horton, D.E., Johnson, N.C., Singh, D., Swain, D.L., Rajaratnam, B., Diffenbaugh, N.S., 2015. Contribution of changes in atmospheric circulation patterns to extreme temperature trends. Nature. 522, 465–469. https://doi.org/10.1038/nature14550.

Jin, D., Guan, Z., Tang, W., 2013. The Extreme Drought Event during Winter-Spring of 2011 in East China: Combined Influences of Teleconnection in Midhigh Latitudes and Thermal Forcing in Maritime Continent Region. J. Clim. 26, 8210–8222. https://doi.org/10.1175/JCLI-D-12-00652.1.

Khoshnazar, A., Corzo Perez, G., Sajjad, M., 2023. Characterizing spatial–temporal drought risk heterogeneities: A hazard, vulnerability and resilience-based modeling. J. Hydrol. 619, 129321 https://doi.org/10.1016/j.jhydrol.2023.129321.

Lin, W., Wen, C., Wen, Z., Gang, H., 2015. Drought in Southwest China: A Review. Atmos. Ocean. Sci. Lett. 8, 339–344. https://doi.org/10.3878/AOSL20150043.

Liu, W.T., Kogan, F.N., 1996. Monitoring regional drought using the Vegetation Condition Index. Int. J. Remote Sens. 17, 2761–2782. https://doi.org/10.1080/01431169608949106.

Liu, Y., Ni, Z., Zhao, Y., Zhou, G., Luo, Y., Li, S., Wang, D., Zhang, S., 2022. Spatial-Temporal Evolution and Driving Forces of Drying Trends on the Qinghai-Tibet Plateau Based on Geomorphological Division. Int. J. Environ. Res. Public Health. 19, 7909. https://doi.org/10.3390/ijerph19137909.

Luo, X., Keenan, T.F., 2022. Tropical extreme droughts drive long-term increase in atmospheric CO2 growth rate variability. Nat. Commun. 13, 1193. https://doi.org/10.1038/s41467-022-28824-5.

Martínez-Fernández, J., González-Zamora, A., Sánchez, N., Gumuzzio, A., 2015. A soil water based index as a suitable agricultural drought indicator. J. Hydrol. 522, 265–273. https://doi.org/10.1016/j.jhydrol.2014.12.051.

McKee, T.B., Doesken, N.J., Kleist, J., 1993. The relationship of drought frequency and duration to time scales. Proceedings of the 8th Conference on Applied Climatology. 17, 179-183.

Mishra, A.K., Singh, V.P., 2010. A review of drought concepts. J. Hydrol. 391, 202–216. https://doi.org/10.1016/j.jhydrol.2010.07.012.

Palmer, W.C., 1965. Meteorological drought. US Department of Commerce Weather Bureau, Washington DC.

Pan, Y., Zhu, Y., Lü, H., Yagci, A.L., Fu, X., Liu, E., Xu, H., Ding, Z., Liu, R., 2023. Accuracy of agricultural drought indices and analysis of agricultural drought characteristics in China between 2000 and 2019. Agric. Water Manage. 283, 108305 https://doi.org/10.1016/j.agwat.2023.108305.

Peng, D., Zhou, T., 2017. Why was the arid and semiarid northwest China getting wetter in the recent decades? J. Geophys. Res.-Atmos. 122, 9060–9075. https://doi.org/10.1002/2016JD026424.

Qin, Z., Tang, H., Li, W., Zhang, H., Zhao, S., Wang, Q., 2014. Modelling impact of agro-drought on grain production in China. Int. J. Disaster Risk Reduct. 7, 109–121. https://doi.org/10.1016/j.ijdrr.2013.09.002.

Rojas, O., Vrieling, A., Rembold, F., 2011. Assessing drought probability for agricultural areas in Africa with coarse resolution remote sensing imagery. Remote Sens. Environ. 115, 343–352. https://doi.org/10.1016/j.rse.2010.09.006.

Sawada, Y., Koike, T., Jaranilla-Sanchez, P.A., 2014. Modeling hydrologic and ecologic responses using a new eco-hydrological model for identification of droughts. Water Resour. Res. 50, 6214–6235. https://doi.org/10.1002/2013WR014847.

Scott, L.M., Janikas, M.V., 2010. Spatial statistics in ArcGIS. Springer, Berlin Heidelberg,. https://doi.org/10.1007/978-3-642-03647-7_2.

Sen, P.K., 1968. Estimates of the regression coefficient based on kendall's tau. J. Am. Stat. Assoc. 63, 1379–1389. https://doi.org/10.1080/01621459.1968.10480934.

Shi, W., Wang, M., Liu, Y., 2021. Crop yield and production responses to climate disasters in China. Sci. Total Environ. 750, 141147 https://doi.org/10.1016/j.scitotenv.2020.141147.

Shi, X., Yang, Y., Ding, H., Chen, F., Shi, M., 2023. Analysis of the Variability characteristics and applicability of SPEI in Mainland China from 1985 to 2018. Atmosphere. 14, 790. https://doi.org/10.3390/atmos14050790.

Srivastava, P.K., 2017. Satellite Soil Moisture: Review of Theory and Applications in Water Resources. Water Resour. Res. 31, 3161–3176. https://doi.org/10.1007/s11269-017-1722-6.

Su, B., Huang, J., Fischer, T., Wang, Y., Kundzewicz, Z.W., Zhai, J., Sun, H., Wang, A., Zeng, X., Wang, G., et al., 2018. Drought losses in China might double between the 1.5 °C and 2.0 °C warming. Proc. Natl. Acad. Sci. u. s. a. 115, 10600–10605. https://doi.org/10.1073/pnas.1802129115.

Vicente-Serrano, S.M., Beguería, S., López-Moreno, J.I., 2010. A multiscalar drought index sensitive to global warming: the standardized precipitation evapotranspiration index. J. Clim. 23, 1696–1718. https://doi.org/10.1175/2009JCLI2909.1.

Wan, L., Bento, V.A., Qu, Y., Qiu, J., Song, H., Zhang, R., Wu, X., Xu, F., Lu, J., Wang, Q., 2023. Drought characteristics and dominant factors across China: Insights from high-resolution daily SPEI dataset between 1979 and 2018. Sci. Total Environ. 901, 166362 https://doi.org/10.1016/j.scitotenv.2023.166362.

Wang, Z., Li, J., Lai, C., Zeng, Z., Zhong, R., Chen, X., Zhou, X., Wang, M., 2017b. Does drought in China show a significant decreasing trend from 1961 to 2009? Sci. Total Environ. 579, 314–324. https://doi.org/10.1016/j.scitotenv.2016.11.098.

Wang, R., Li, L., Gentine, P., Zhang, Y., Chen, J., Chen, X., Chen, L., Ning, L., Yuan, L., Lü, G., 2022. Recent increase in the observation-derived land evapotranspiration due to global warming. Environ. Res. Lett. 17, 024020 https://doi.org/10.1088/1748-9326/ac4291.

Wang, X., Luo, P., Zheng, Y., Duan, W., Wang, S., Zhu, W., Zhang, Y., Nover, D., 2023. Drought disasters in China from 1991 to 2018: analysis of spatiotemporal trends and characteristics. Remote Sens. 15, 1708. https://doi.org/10.3390/rs15061708.

Wang, S., Yuan, X., Li, Y., 2017a. Does a strong el niño imply a higher predictability of extreme drought? Sci Rep. 7, 40741. https://doi.org/10.1038/srep40741.

Wang, Q., Zeng, J., Qi, J., Zhang, X., Zeng, Y., Shui, W., Xu, Z., Zhang, R., Wu, X., Cong, J., 2021. A multi-scale daily SPEI dataset for drought characterization at observation stations over mainland China from 1961 to 2018. Earth Syst. Sci. Data. 13, 331–341. https://doi.org/10.5194/essd-13-331-2021.

Wu, Z., Huang, N.E., 2004. A study of the characteristics of white noise using the empirical mode decomposition method. Proc. R Soc. London Ser. A-Math. Phys. Eng. Sci. 460, 1597–1611. https://doi.org/10.1098/rspa.2003.1221.

Wu, Z., Huang, N.E., 2009. Ensemble empirical mode decomposition: a noise-assisted data analysis method. Adv. Adapt. Data Anal. 1, 1–41. https://doi.org/10.1142/S1793536909000047.

Wu, Z., Yu, L., Du, Z., Zhang, H., Fan, X., Lei, T., 2020. Recent changes in the drought of China from 1960 to 2014. Int. J. Climatol. 40, 3281–3296. https://doi.org/10.1002/joc.6397.

Yang, B., Cui, Q., Meng, Y., Zhang, Z., Hong, Z., Hu, F., Li, J., Tao, C., Wang, Z., Zhang, W., 2023. Combined multivariate drought index for drought assessment in China from 2003 to 2020. Agric. Water Manage. 281, 108241 https://doi.org/10.1016/j.agwat.2023.108241.

Yao, N., Li, Y., Lei, T., Peng, L., 2018. Drought evolution, severity and trends in mainland China over 1961–2013. Sci. Total Environ. 616–617, 73–89. https://doi.org/10.1016/j.scitotenv.2017.10.327.

Yevjevich, V.M., 1967. An objective approach to definitions and investigations of continental hydrologic droughts. Colorado State University, Fort Collins.

Yin, J., Gentine, P., Slater, L., Gu, L., Pokhrel, Y., Hanasaki, N., Guo, S., Xiong, L., Schlenker, W., 2023. Future socio-ecosystem productivity threatened by compound drought–heatwave events. Nat. Sustain. 6, 259–272. https://doi.org/10.1038/s41893-022-01024-1.

Yu, M., Li, Q., Hayes, M.J., Svoboda, M.D., Heim, R.R., 2014. Are droughts becoming more frequent or severe in China based on the Standardized Precipitation Evapotranspiration Index: 1951–2010? Int. J. Climatol. 34, 545–558. https://doi.org/10.1002/joc.3701.

Yu, H., Zhang, Q., Xu, C.-Y., Du, J., Sun, P., Hu, P., 2019. Modified palmer drought severity index: model improvement and application. Environ. Int. 130, 104951 https://doi.org/10.1016/j.envint.2019.104951.

Zeng, J., Li, Z., Chen, Q., Bi, H., Qiu, J., Zou, P., 2015. Evaluation of remotely sensed and reanalysis soil moisture products over the Tibetan Plateau using in-situ observations. Remote Sens. Environ. 163, 91–110. https://doi.org/10.1016/j.rse.2015.03.008.

Zeng, Z., Wu, W., Li, Y., Zhou, Y., Zhang, Z., Zhang, S., Guo, Y., Huang, H., Li, Z., 2020. Spatiotemporal Variations in Drought and Wetness from 1965 to 2017 in China. Water. 12, 2097. https://doi.org/10.3390/w12082097.

Zhai, J., Huang, J., Su, B., Cao, L., Wang, Y., Jiang, T., Fischer, T., 2017. Intensity–area–duration analysis of droughts in China 1960–2013. Clim. Dyn. 48, 151–168. https://doi.org/10.1007/s00382-016-3066-y.

Zhang, X., Chen, N., Li, J., Chen, Z., Niyogi, D., 2017. Multi-sensor integrated framework and index for agricultural drought monitoring. Remote Sens. Environ. 188, 141–163. https://doi.org/10.1016/j.rse.2016.10.045.

Zhang, W., Jin, F.-F., Zhao, J.-X., Qi, L., Ren, H.-L., 2013. The possible influence of a nonconventional el niño on the severe autumn drought of 2009 in Southwest China. J. Clim. 26, 8392–8405. https://doi.org/10.1175/JCLI-D-12-00851.1.

Zhang, Y., Wu, Z., Singh, V.P., Lin, Q., Ning, S., Zhou, Y., Jin, J., Zhou, R., Ma, Q., 2023. Agricultural drought characteristics in a typical plain region considering irrigation, crop growth, and water demand impacts. Agric. Water Manage. 282, 108266 https://doi.org/10.1016/j.agwat.2023.108266.

Zhang, L., Xiao, J., Li, J., Wang, K., Lei, L., Guo, H., 2012. The 2010 spring drought reduced primary productivity in southwestern China. Environ. Res. Lett. 7, 045706 https://doi.org/10.1088/1748-9326/7/4/045706.

Zhang, Q., Yu, H., Sun, P., Singh, V.P., Shi, P., 2019. Multisource data based agricultural drought monitoring and agricultural loss in China. Glob. Planet. Change. 172, 298–306. https://doi.org/10.1016/j.gloplacha.2018.10.017.

Zhang, Q., Yao, Y., Li, Y., Huang, J., Ma, Z., Wang, Z., Wang, S., Wang, Y., Zhang, Y., 2020. Progress and prospect on the study of causes and variation regularity of droughts in China. Acta Meteorol. Sin. 78, 500–521. https://doi.org/10.11676/qxxb2020.032.

Zhao, R., Sun, H., Xing, L., Li, R., Li, M., 2023. Effects of anthropogenic climate change on the drought characteristics in China: from frequency, duration, intensity, and affected area. J. Hydrol. 617, 129008 https://doi.org/10.1016/j.jhydrol.2022.129008.

Zhou, J., Li, Q., Wang, L., Lei, L., Huang, M., Xiang, J., Feng, W., Zhao, Y., Xue, D., Liu, C., et al., 2019. Impact of Climate Change and Land-Use on the Propagation from Meteorological Drought to Hydrological Drought in the Eastern Qilian Mountains. Water. 11, 1602. https://doi.org/10.3390/w11081602.